IVYSPRING INTERNATIONAL PUBLISHER

Theranostics

2027; 17(1): 671-696. doi: 10.7150/thno.134479

Research Paper

A long-acting naltrexone microsphere, IVL4002, ameliorates experimental autoimmune encephalomyelitis by attenuating TLR4-associated neuroinflammation and blood–brain barrier dysfunction

Tae Woo Kwon[1,2†], Soyoung Youm[3†], Hyo-Sung Jo[1,2], Yujeong Ha[1,2], Da Yeon Park[2,4], Slgirim Lee[3], Yooyoung Lee[3], Jooyoung Cha[3], Juhee Kim[3✉], and Ik-Hyun Cho[1,2,4✉]

1. Department of Convergence Medical Science, College of Korean Medicine, Kyung Hee University, Seoul, 02447, Republic of Korea.
2. Department of Science in Korean Medicine, Graduate School, Kyung Hee University, Seoul, 02447, Republic of Korea.
3. Inventage Lab Inc., Bundang-gu, Seongnam-si, 13494, Gyeonggi-do, Republic of Korea.
4. KHU-KIST Department of Converging Science and Technology, Kyung Hee University, Seoul, 02447, Republic of Korea.

†These authors contributed equally to this work.

✉ Corresponding authors: Juhee Kim, Inventage Lab Inc., Bundang-gu, Seongnam-si, Gyeonggi-do 13494, Republic of Korea. Tel: +82-31-605-5130; Fax: +82-31-605-5136; E-mail: jade@inventagelab.com; ORCID ID: 0000-0003-4778-3041. Ik-Hyun Cho, DVM, Ph.D., Department of Convergence Medical Science, College of Korean Medicine, Kyung Hee University, Seoul, 02447, Republic of Korea. Tel: +82-2-961-0749; Fax: +82-2-965-5969; E-mail: ihcho@khu.ac.kr; ORCID ID: 0000-0002-3868-7384.

© 2027 The Author(s). This is an open access article distributed under the Creative Commons Attribution 4.0 International Licence, subject to the Publisher's Terms of Use at https://ivyspring.com/terms.

Received: 2026.03.15; Accepted: 2026.10.08; Published: 2027.01.01

Abstract

Background: Multiple sclerosis (MS) involves immune-mediated demyelination and neurodegeneration, together with impairment of blood–brain barrier (BBB) function. Current disease-modifying therapies effectively reduce relapses but provide limited control over persistent CNS innate immune activation and neurovascular injury. We therefore investigated the therapeutic activity and underlying mechanisms of IVL4002, a DrugFluidics®-manufactured, sustained-release microsphere formulation of naltrexone, in experimental autoimmune encephalomyelitis (EAE).

Methods: EAE mice received a single subcutaneous administration of IVL4002 at 3 days after immunization. Clinical severity, motor function, spinal cord demyelination, inflammatory cell infiltration, and glial activation were assessed. Peripheral immune responses were evaluated by analyzing lymphoid organ hypertrophy and $CD4^+$ T-cell subsets. Mechanistic analyses examined activation of the TLR4/MyD88/NF-κB/MAPKs signaling pathway in the spinal cord. Complementary *in vitro* studies were conducted in BV2 microglial and bEnd.3 endothelial cells to evaluate naltrexone-mediated regulation of TLR4-dependent inflammatory signaling and endothelial activation.

Results: IVL4002 significantly ameliorated clinical severity, motor dysfunction, and lumbar spinal cord demyelination in EAE mice. Maximal efficacy was observed at an intermediate dose (1 mg/head), which maintained plasma naltrexone concentrations within an optimal exposure range, whereas higher doses conferred no additional benefit. Within this therapeutic window, IVL4002 reduced inflammatory cell infiltration, microglial and astrocytic activation, and pro-inflammatory mediator expression in the spinal cord. It also suppressed lymphoid organ hypertrophy, limited pathogenic $CD4^+$ Th1 and Th17 cell expansion, and reduced their CNS infiltration without broad immunosuppression. Mechanistically, IVL4002 inhibited activation of the TLR4/MyD88/NF-κB/MAPKs signaling cascade. *In vitro*, naltrexone suppressed LPS-induced TLR4-dependent inflammatory signaling in microglia and endothelial cells.

Conclusions: Maintaining naltrexone exposure within an effective systemic exposure range was associated with coordinated suppression of peripheral pathogenic T-cell responses, CNS innate immune activation, and BBB dysfunction, supporting IVL4002 as a promising long-acting drug-repurposing strategy for MS.

Keywords: multiple sclerosis, experimental autoimmune encephalomyelitis, sustained-release naltrexone, long-acting microsphere, TLR4 signaling, neuroinflammation, blood–brain barrier

Introduction

Multiple sclerosis (MS) is driven by immune-mediated injury within the central nervous system (CNS), resulting in myelin loss, axonal damage, and progressive neurological impairment [1-3]. Peripheral autoreactive lymphocytes contribute substantially to CNS inflammation, while persistent innate immune activation within the CNS, BBB dysfunction, and impaired tissue repair mechanisms are increasingly recognized as important contributors to disease progression [1, 4]. These processes collectively promote neurodegeneration and contribute to the progression of MS, although no single experimental model fully recapitulates the heterogeneous clinical and pathological features of the disease.

Many disease-modifying therapies (DMTs) reduce relapses and radiological disease activity through effects on lymphocyte trafficking, proliferation, or differentiation. Nevertheless, treatment-related adverse effects and the burden of repeated dosing can hinder long-term adherence [5, 6]. Although many currently approved DMTs primarily modulate peripheral adaptive immunity, persistent innate immune activation within the CNS and BBB dysfunction remain important therapeutic challenges. These processes contribute to ongoing tissue injury and disease progression, highlighting the need for complementary therapeutic approaches [1-3].

BBB disruption is a hallmark pathological feature of MS and actively contributes to disease pathogenesis. Structural and functional alterations of the neurovascular unit facilitate immune cell infiltration, amplify cytokine diffusion, and sustain a pro-inflammatory microenvironment within the CNS [2]. Microglia can support debris removal and tissue recovery under physiological conditions; however, prolonged microglial activation sustains inflammatory signaling and may aggravate synaptic and axonal injury [3]. Persistent microglial responses and BBB disruption may thus reinforce one another and promote chronic CNS pathology.

Toll-like receptor 4 (TLR4) signaling has emerged as a central molecular pathway linking innate immune activation, BBB dysfunction, and adaptive immune amplification in MS and experimental autoimmune encephalomyelitis (EAE). Activation of TLR4 in microglia, infiltrating macrophages, astrocytes, and endothelial cells triggers MyD88-dependent signaling cascades leading to activation of nuclear factor-κB (NF-κB) and mitogen-activated protein kinases (MAPKs), including extracellular signal-regulated kinase (ERK), c-Jun NH2-terminal kinase (JNK), and p38 [7-9]. These pathways induce pro-inflammatory mediators such as inducible nitric oxide synthase (iNOS), interleukin-6 (IL-6), and chemokines that promote pathogenic Th1 and Th17 responses. Elevated TLR4 activity in both human MS lesions and EAE models correlates with glial activation, BBB permeability, and immune cell infiltration, highlighting TLR4 as an attractive therapeutic target for neuroinflammation [7-10].

Naltrexone, a μ-opioid receptor (MOR) antagonist approved for the treatment of opioid and alcohol dependence, has a well-established clinical safety profile [11]. Beyond its canonical opioid receptor antagonism, accumulating evidence suggests that (+)-naltrexone and related stereoisomers function as antagonists of the myeloid differentiation factor-2 (MD-2)/TLR4 complex, thereby inhibiting TLR4-dependent inflammatory signaling independently of opioid receptor blockade [12]. In microglial and macrophage models, naltrexone suppresses lipopolysaccharide-induced NF-κB and MAPK activation and reduces pro-inflammatory mediator production [13].

Low-dose naltrexone (3–5 mg/day) has therefore attracted attention as an alternative therapeutic approach in immune-related disorders including MS [14, 15]. Clinical observations have suggested potential improvements in fatigue, spasticity, and quality of life in MS patients treated with low-dose naltrexone [16, 17]. However, randomized clinical trials have produced inconsistent outcomes [18]. These discrepancies may partly reflect unstable systemic drug exposure associated with oral dosing and the difficulty of maintaining drug levels within a therapeutically effective range.

IVL4002 is a long-acting injectable formulation in which naltrexone is incorporated into biodegradable poly(lactic-co-glycolic acid) (PLGA) microspheres using the proprietary IVL-DrugFluidic® microfluidic platform [19]. PLGA has been widely adopted in sustained-release formulations because its degradation and drug-release properties can be adjusted according to formulation requirements [19, 20]. The microfluidic manufacturing process provides controlled particle formation, supporting consistent and prolonged naltrexone exposure while limiting excessive initial drug release.

In the present study, we investigated the therapeutic efficacy and mechanistic actions of IVL4002 using the myelin oligodendrocyte glycoprotein (MOG_{35-55})-induced EAE model in C57BL/6 mice, a well-established model that reproducibly recapitulates key pathological features of MS, including T cell-mediated neuroinflammation, demyelination, glial activation, BBB dysfunction, and neurological deficits, although it does not fully reproduce the heterogeneous clinical courses of

human MS. Specifically, we characterize its pharmacokinetic profile and safety of IVL4002, define the effective *in vivo* exposure range, and determine whether sustained delivery of naltrexone suppresses TLR4/NF-κB/MAPK signaling, limits pathogenic $CD4^+$ Th1 and Th17 responses, reduces glial activation and macrophage infiltration, and preserves BBB integrity.

Materials and Methods

IVL4002, a naltrexone-encapsulating microsphere formulation

IVL4002 was manufactured using the IVL-DrugFluidic® platform, a parallelized microfluidic system designed for uniform droplet generation. Naltrexone and biodegradable PLGA were incorporated into an organic phase, which was introduced together with an aqueous phase into multichannel microfluidic chips at controlled flow rates to generate uniform droplets (Figure 1A). The resulting droplets were subjected to solvent extraction and drying to produce solid microspheres. The optimized naltrexone-loaded microsphere formulation was designated IVL4002. Before administration, the microspheres were dispersed in an injectable vehicle containing D-mannitol, sodium carboxymethylcellulose, and water for injection.

Characterization of naltrexone-loaded microspheres

Microsphere morphology was visualized by scanning electron microscopy using an SNE-3000M instrument (SEC Co., Ltd., Suwon, Republic of Korea). Size distribution was measured with an S3550 laser particle size analyzer (Microtrac Inc., Montgomeryville, PA, USA) and summarized using the D50 and span values. To determine encapsulation efficiency, the microspheres were dissolved in an organic solvent and their naltrexone content was measured by HPLC using the e2695 system coupled to a 2998 PDA detector (Waters Corp., Milford, MA, USA). Residual solvents were quantified separately by gas chromatography using a YL6500 system. Encapsulation efficiency (%) was calculated using the following equation:

$$Encapsulation\ efficiency\ (\%) = \frac{Actual\ naltrexone\ content}{Theoretical\ naltrexone\ content} \times 100$$

Animals and ethical approval

Male ICR (CD-1) mice used for the pharmacokinetic (PK) study and male and female Sprague–Dawley (SD) rats used for the toxicity study were obtained from Koatech Co., Ltd. (Pyeongtaek, Republic of Korea), with breeding colonies derived from seed animals originating from Charles River Laboratories, Inc. (Raleigh, NC, USA). All rodents were 8 weeks old at the time of dosing and underwent an acclimation period of at least 1 week before treatment. Rodents were housed under standardized environmental conditions (temperature 23 ± 2 °C, relative humidity 55 ± 5%) with a 12-h light/dark cycle (lights on from 08:00 to 20:00). Standard laboratory chow and water were provided *ad libitum*. The mouse PK study was conducted at HLB BioStep Co., Ltd. (Incheon, Republic of Korea) and approved by its Institutional Animal Care and Use Committee (IACUC; approval no. 25-HB-0017), whereas the rat toxicity study was conducted under Good Laboratory Practice (GLP) regulations at IIT Research Institute (IITRI; Chicago, IL, USA) and approved by the IITRI IACUC (approval no. 311900100201).

Male and female beagle dogs (Ridglan Farms, Wisconsin, USA), aged 7–8 months at the time of dosing, were used for the toxicity study. Animals were housed under controlled environmental conditions (temperature, 18–29 °C; relative humidity, 30–70%) with a 12-h light/dark cycle. Approximately 400 g of feed was provided daily for at least 2 h, and municipal drinking water (City of Chicago) was available *ad libitum* through an automatic watering system. The dog toxicity study was conducted at IIT Research Institute (IITRI; Chicago, IL, USA) and was approved by the IITRI Institutional Animal Care and Use Committee (IACUC; approval no. 311900100301).

For the EAE study, eight- to nine-week-old female C57BL/6 mice (19–21 g) were obtained from Koatech Co., Ltd. (Pyeongtaek, Republic of Korea). Animals were acclimated for 7 days before experimental procedures and housed under controlled environmental conditions (temperature, 23 ± 2 °C; relative humidity, 55 ± 5%; 12-h light/dark cycle, lights on from 08:00 to 20:00) with *ad libitum* access to food and water. The EAE study was approved by the Institutional Animal Care and Use Committee (IACUC) of Kyung Hee University (approval no. KHUASP(SE)-23-560). Animals were randomly assigned to experimental groups, and investigators performing clinical scoring, histological evaluation, and data analysis were blinded to treatment allocation. Randomization and blinding were implemented in accordance with recommendations from the National Institute of Neurological Disorders and Stroke (NINDS) workshop on preclinical models of neurological disease [21]

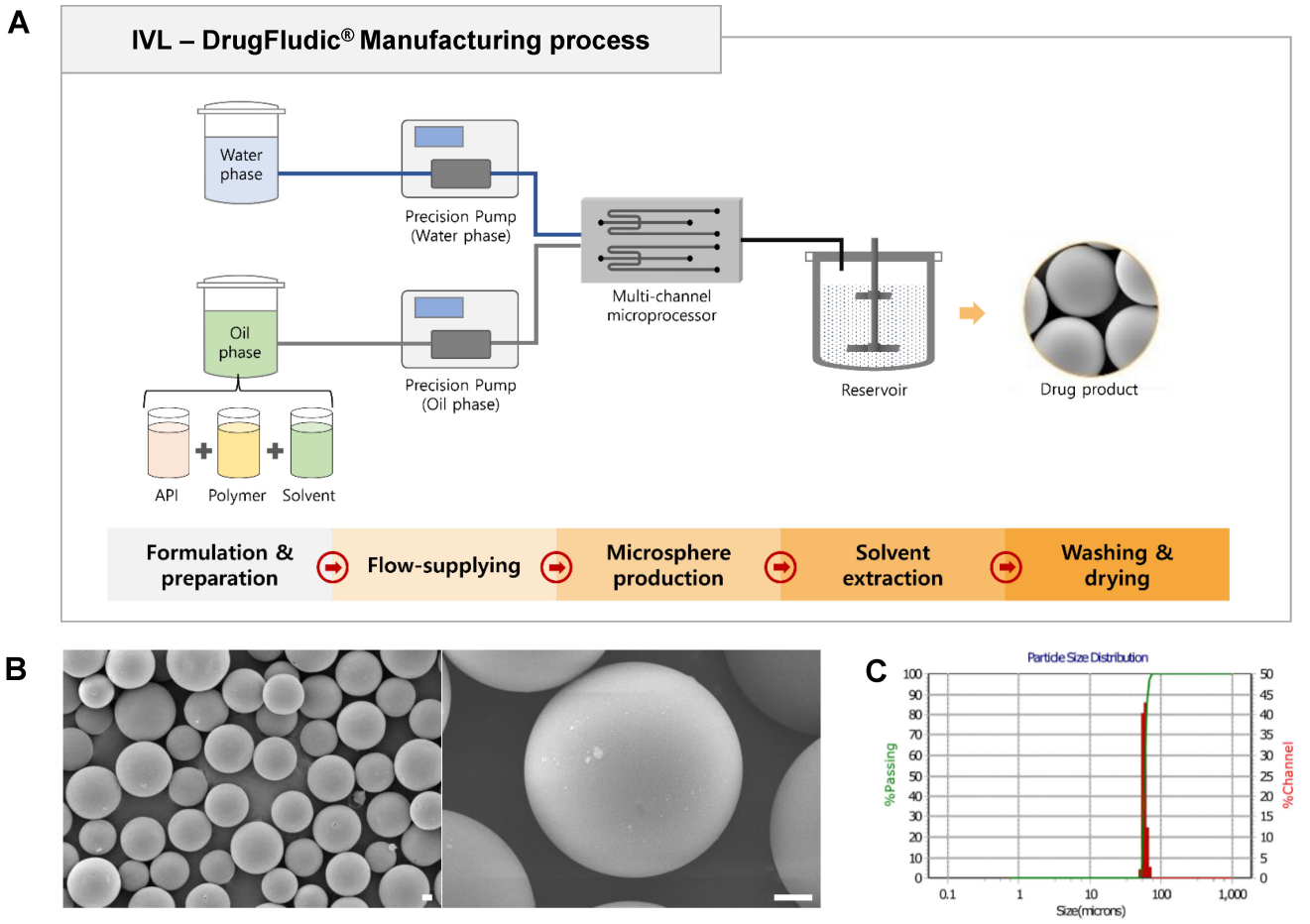


Figure 1. Manufacturing process and characterization of naltrexone-loaded PLGA microspheres (IVL4002). (A) Schematic illustration of the IVL-DrugFluidic® microfluidic manufacturing process used to produce IVL4002. The aqueous phase and oil phase containing PLGA and naltrexone were delivered by precision pumps into a multi-channel microprocessor to generate monodisperse droplets, followed by solvent extraction, washing, and drying. **(B)** Representative scanning electron microscopy (SEM) images of IVL4002 microspheres, showing uniform spherical morphology with smooth surfaces. Scale bar, 10 μm. **(C)** Particle-size distribution of IVL4002 microspheres determined by laser diffraction analysis.

Pharmacokinetic study

A PK study was conducted to characterize systemic exposure to naltrexone following a single subcutaneous administration of IVL4002. Male ICR (CD-1) mice received IVL4002 at doses of 0.2, 1, or 10 mg/head (n = 4 per group). Approximately 80 μL of blood was collected from the jugular vein at predetermined time points (8, 24, 48, 72, 120, 168, 336, 504, 672, and 840 h post-injection). Plasma was separated immediately by centrifugation (13,000 rpm, 2 min, 4 °C) and stored at −80 °C until analysis. Plasma naltrexone concentrations were quantified using liquid chromatography–tandem mass spectrometry (LC–MS/MS; Shimadzu LC-40 system coupled with a SCIEX Triple Quad 7500 mass spectrometer, Framingham, MA, USA). The bioanalytical method was validated according to standard regulatory guidelines, with calibration standards and quality control samples included in each analytical batch to ensure assay accuracy and precision. The lower limit of quantification (LLOQ) for naltrexone was 0.1 ng/mL, and the intra- and inter-day accuracy and precision met the predefined acceptance criteria.

Toxicity studies

Toxicity studies of IVL4002 were conducted in rats and dogs under GLP conditions to evaluate systemic and local tolerability.

Rat study: Rats were randomly assigned to four groups (n = 10 males and 10 females per group): saline control, placebo control, IVL4002 single-dose, and IVL4002 repeated-dose groups. The placebo formulation consisted of naltrexone-free microspheres suspended in the vehicle. IVL4002 was administered subcutaneously at a fixed dose of 37.5 mg/head. The single-dose group received IVL4002 on Day 1, whereas the repeated-dose group received IVL4002 on Days 1, 15, and 29. Clinical observations, body weight, food consumption, and clinical pathology parameters were evaluated according to the study schedule. At scheduled necropsy, animals underwent gross pathological examination, followed by

histopathological evaluation of major organs and tissues.

Dog study: Dogs were allocated to four treatment groups (n = 3 males and 3 females per group): saline control, placebo control, IVL4002 single-dose, and IVL4002 repeated-dose groups. IVL4002 was administered subcutaneously at 37.5 mg/head according to the designated dosing schedule. Clinical observations, body weight, food consumption, clinical pathology parameters, and organ weights were evaluated according to the study schedule. Gross pathological and histopathological examinations were performed at scheduled necropsy.

Injection-site histopathology: Injection-site tissues were collected at scheduled necropsy from the rat and dog GLP toxicity studies, fixed in 10% neutral-buffered formalin, paraffin-embedded, sectioned, and stained with hematoxylin and eosin (H&E) as previously described [22, 23]. Histopathological evaluation was performed to assess local tissue responses, including inflammation, foreign-body reactions, hemorrhage, necrosis, and other treatment-related pathological changes.

Experimental design, treatment groups, and treatment for EAE

Mice were randomly divided into the following treatment conditions/groups at 3 days after immunization: (1) Sham, which received no myelin oligodendrocyte glycoprotein (MOG_{35-55}) immunization and was administered saline subcutaneously (s.c.); (2) EAE + vehicle, which received MOG_{35-55} immunization (*s.c.*) and the formulation vehicle (D-mannitol, sodium carboxymethylcellulose, and water for injection) administered subcutaneously; (3) EAE + IVL4002, which received MOG_{35-55} immunization (*s.c.*) and IVL4002 (*s.c.*) at concentrations of 0.2, 1, or 10 mg/head; (4) EAE + Teriflunomide, which received MOG_{35-55} immunization (*s.c.*) and Teriflunomide (3 mg/kg, *p.o.*); (5) EAE + dimethyl fumarate (DMF), which received MOG_{35-55} immunization (*s.c.*) and DMF (100 mg/kg, p.o.); (6) IVL4002 only, which did not receive MOG_{35-55} immunization but was administered IVL4002 (1 mg/head, *s.c.*). IVL4002 was suspended in the formulation vehicle and administered as a single subcutaneous injection at 3 days after immunization using a 1-mL syringe fitted with a 25-G needle. Mice in the EAE + vehicle group received an equal volume of the same vehicle without IVL4002. The doses used in the present study were selected based on a preliminary dose-finding study (Figure S2), in which 1 mg/head showed the greatest therapeutic efficacy among the doses evaluated (1, 5, and 10 mg/head). Accordingly, 1 mg/head was selected for subsequent efficacy and mechanistic studies, while 0.2 mg/head was additionally included to evaluate the lower end of the dose range.

To investigate whether MOR antagonism contributes to the bell-shaped dose–response relationship of IVL4002, methylnaltrexone (MNTX), a peripherally restricted MOR antagonist, was used. Mice were divided into the following groups: EAE, EAE + IVL4002 (1 mg/head), EAE + IVL4002 (10 mg/head), EAE + IVL4002 (1 mg/head) + MNTX, EAE + IVL4002 (10 mg/head) + MNTX, and EAE + MNTX. IVL4002 was administered as a single subcutaneous injection 3 days after immunization, whereas MNTX (3 mg/kg, *s.c.*) was administered once daily, beginning 2 h before IVL4002 administration and continuing until the end of the experiment. MNTX was prepared in water for injection [24, 25].

EAE induction and clinical assessment

EAE was established using a previously reported protocol [23]. Each mouse received a subcutaneous injection into both hind flanks of 100 µL emulsion containing MOG35-55 peptide (100 µg) and CFA supplemented with 500 µg of M. tuberculosis H37Ra. PTX (200 ng in 100 µL PBS, i.p.) was given immediately after immunization and again 2 days later. Neurological signs were assessed daily on a 0–7 scale: 0, no signs; 1, partial tail weakness; 2, complete tail paralysis; 3, impaired hind-limb gait with tail paralysis; 4, complete hind-limb paralysis; 5, paraplegia with partial forelimb involvement; 6, tetraplegia or moribund condition; and 7, death. Mice exhibiting severe paralysis or a moribund condition were euthanized according to humane endpoint criteria approved by the IACUC.

Histopathological analysis

Histopathological examinations were conducted in accordance with previously published methods [22]. At the peak of clinical disease (16–17 days post-immunization), mice were deeply anesthetized with isoflurane and transcardially perfused with 0.9% saline, followed by 4% paraformaldehyde (PFA) in 0.1 M phosphate buffer (pH 7.4). Lumbar spinal cord segments (L4–L6) were carefully isolated, post-fixed in 4% PFA for 48 h, and cryoprotected overnight in 30% sucrose solution. Following cryoprotection, tissues were embedded in optimal cutting temperature (OCT) compound (Tissue-Tek, Sakura Finetek Co., Ltd., Japan) and snap-frozen in liquid nitrogen. Coronal spinal cord sections were cut at a thickness of 10 µm using a cryostat and mounted onto glass slides coated with 1% gelatin. Spinal cord sections were subjected to H&E and Luxol Fast Blue (LFB) staining according to established protocols [22, 23]. For H&E staining,

sections were stained with H&E to assess inflammatory cell infiltration and overall tissue pathology. For LFB staining, sections were stained with LFB solution and differentiated to visualize myelinated white matter and assess the extent of demyelination. After staining, sections were sequentially dehydrated through graded ethanol solutions, cleared in xylene, and coverslipped using Permount mounting medium (VWR International, LLC, Mississauga, Canada). Histological images were acquired using a BX50 light microscope (Olympus, Tokyo, Japan) equipped with an eXcope T300 digital imaging system (DIXI Science, Daejeon, Republic of Korea).

Histological scoring and quantitative analysis

Inflammatory cell infiltration assessed by H&E staining was graded using the following scale [23]: 0, no detectable lesions; 1, inflammatory infiltration confined to the meninges; 2, focal and superficial parenchymal infiltration; 3, moderate infiltration involving < 25% of the white matter; 4, extensive infiltration involving 25–50% of the white matter; and 5, severe infiltration involving > 50% of the white matter. Demyelination assessed by LFB staining was graded according to a previously described scoring system [26]: 0, no demyelination; 1, focal demyelination involving ≤ 25% of the white matter; 2, moderate demyelination involving 26–50% of the white matter; and 3, severe and diffuse demyelination involving > 50% of the white matter. Quantitative image analyses were performed using ImageJ software (National Institutes of Health, Bethesda, MD, USA). All histological evaluations and quantitative analyses were performed by investigators blinded to the treatment groups.

Blood–brain barrier permeability assay

BBB permeability was assessed at the peak stage of EAE using an Evans Blue extravasation assay, as previously described with minor modifications [27]. Mice were administered 2% Evans Blue (4 mL/kg) intravenously via the retro-orbital route. Two hours after dye administration, mice were anesthetized and transcardially perfused with cold PBS to remove intravascular Evans Blue. The brain and spinal cord were immediately harvested, and images were acquired under identical conditions to assess Evans Blue distribution. For quantitative analysis, the wet weight of the harvested brain was measured, and the tissue was homogenized in 50% trichloroacetic acid (TCA) at a ratio of 2 mL per 1 g of tissue. The homogenates were incubated for 15 min and centrifuged at 15,000 × g for 20 min at 4 °C. The supernatants were carefully collected, and 30 µL of each supernatant was transferred to a 96-well plate and mixed with 90 µL of 95% ethanol. Evans Blue fluorescence was measured using a microplate reader at an excitation wavelength of 620 nm and an emission wavelength of 680 nm. Evans Blue extravasation was quantified using a standard curve prepared under identical solvent conditions and expressed as µg of Evans Blue per mg of wet tissue according to the following equation:

$$Evans\ Blue\ extravasation\ (\mu g/mg\ tissue) = \frac{C\ (\mu g/mL) \times V(mL) \times DF}{Tissue\ weight\ (mg)}$$

where C is the Evans Blue concentration calculated from the standard curve (µg/mL), V is the total volume of 50% TCA used for tissue extraction (mL), DF is the dilution factor, and tissue weight is the wet tissue weight (mg). For histological assessment, the harvested lumbar spinal cord was cryosectioned at a thickness of 10 µm as described above. Evans Blue fluorescence was examined using a confocal laser-scanning microscope (LSM 7 PASCAL; Carl Zeiss, Oberkochen, Germany), and fluorescence intensity was quantified using ImageJ software.

Immunofluorescence staining

Immunofluorescence (IF) staining was conducted according to previously established protocols [28]. Briefly, frozen sections of the lumbar spinal cord (L4–L6) were prepared from mice in each experimental group at the peak of disease (16–17 days post-immunization; n = 6 per group). Tissue sections were incubated in a blocking solution containing 2% fetal bovine serum (FBS), 2% bovine serum albumin (BSA), 5% normal goat serum, and 0.1% Triton X-100 (Sigma-Aldrich) in PBS for 2 h at room temperature. Following blocking, sections were incubated overnight at 4 °C with primary antibodies against myelin basic protein (MBP), ionized calcium-binding adapter molecule 1 (Iba-1), glial fibrillary acidic protein (GFAP), albumin (ALB), platelet endothelial cell adhesion molecule-1 (PECAM-1), claudin-5 (CLDN5), occludin (OCLN), and zonula occludens-1 (ZO-1) (Table S1). To evaluate the spatial distribution of infiltrating Th1 and Th17 cells, lumbar spinal cord sections were additionally co-immunostained with antibodies against CD4 and IFN-γ or CD4 and IL-17A, respectively (Table S1). After thorough washing, sections were incubated for 1 h at room temperature with appropriate Cy3- or FITC-conjugated secondary antibodies against mouse, rabbit, or rat IgG (1:1,000; Jackson ImmunoResearch, West Grove, PA, USA) (Table S1). Immunolabeled sections were examined using a confocal laser scanning microscope (LSM 7 PASCAL; Carl Zeiss, Oberkochen, Germany). Parenchymal ALB

immunoreactivity was assessed as an indicator of vascular leakage. Fluorescence intensities of ALB and the indicated BBB-associated markers were quantified using ImageJ under identical imaging conditions by investigators blinded to the treatment groups.

Western blot analysis

Western blot analysis was conducted according to established procedures with minor modifications [29]. At the peak of clinical disease (16–17 days post-immunization), lumbar spinal cord tissues (L4–L6) were collected from each experimental group (n = 6 per group). Tissue samples were homogenized on ice using a bead-based homogenizer with zirconium oxide beads in lysis buffer containing 10 mM Tris–HCl (pH 7.4), 0.5 mM EDTA, 0.25 M sucrose, and a protease inhibitor cocktail [28]. Total protein concentrations were determined using a commercial protein assay kit (Sigma-Aldrich). Equal amounts of protein were mixed with SDS sample buffer containing 10% β-mercaptoethanol, denatured at 100 °C for 10 min, and separated by SDS–polyacrylamide gel electrophoresis. Proteins were subsequently transferred onto polyvinylidene difluoride membranes (MilliporeSigma, Burlington, MA, USA) using a semi-dry transfer system (Bio-Rad, Hercules, CA, USA). Membranes were blocked for 1 h at room temperature with 5% bovine serum albumin (BSA) in PBS containing 0.1% Tween-20 (PBST) and incubated overnight at 4 °C with the appropriate primary antibodies (Table S2). After washing with PBST, membranes were incubated for 1 h at room temperature with horseradish peroxidase (HRP)-conjugated secondary antibodies (1:1,000; Jackson ImmunoResearch, West Grove, PA, USA) diluted in 1.5% BSA/PBST (Table S2). Immunoreactive bands were visualized using an enhanced chemiluminescence reagent (BioD., Ltd., Seoul, Republic of Korea) and captured using a Davinci-K Gel Imaging System (CoreBio, Seoul, Republic of Korea). Band intensities were quantified using ImageJ software (National Institutes of Health, Bethesda, MD, USA). Protein expression levels were normalized to β-actin as a loading control, whereas phosphorylated NF-κB, ERK, JNK, and p38 levels were normalized to their corresponding total protein levels. Quantitative data are expressed as relative optical density values.

Reverse transcription–polymerase chain reaction (RT-PCR)

RT-PCR was performed according to previously established protocols with minor modifications [26]. At the peak stage of EAE (16–17 days post-immunization), lumbar spinal cord segments (L4–L6) were rapidly excised and snap-frozen for subsequent RNA isolation. Total RNA was extracted using TRIsure reagent (Bioline, UK) according to the manufacturer's instructions. For complementary DNA (cDNA) synthesis, 1 μg of total RNA was reverse-transcribed at 37 °C for 1 h in a reaction mixture containing oligo(dT) primers (0.5 μg), dNTPs (0.5 mM), 5× first-strand buffer, RNaseOUT ribonuclease inhibitor, dithiothreitol (5 mM), and M-MLV reverse transcriptase (Thermo Fisher Scientific). The sequences of the gene-specific primers used in this study are provided in Table S3. PCR amplification was performed using lumbar spinal cord-derived cDNA, gene-specific primers (5 pmol), and EconoTaq DNA polymerase (0.6 U) in a final reaction volume of 20 μL containing PCR Master Mix (Lucigen, WI, USA). Amplified PCR products were separated by agarose gel electrophoresis and visualized under ultraviolet illumination. Band intensities were quantified and normalized to glyceraldehyde-3-phosphate dehydrogenase (GAPDH) as an internal control. All RT-PCR reactions were performed in triplicate to ensure reproducibility.

Flow cytometry

At the peak stage of EAE (16–17 days post-immunization), mice were deeply anesthetized with isoflurane and euthanized, after which the lumbar spinal cords (L4-L6) and draining lymph nodes were harvested. Immune cell profiling was performed using single-cell suspensions prepared from whole tissues according to previously established protocols [22]. For spinal cord samples, mice were transcardially perfused with cold PBS before tissue collection to minimize contamination by intravascular blood cells. Spinal cord tissues were mechanically dissociated and passed through a 70-μm cell strainer, and mononuclear cells were isolated using a 30%/70% Percoll density gradient. Draining lymph nodes were mechanically dissociated and passed through a 70-μm cell strainer to obtain single-cell suspensions. For intracellular cytokine analysis, isolated cells were stimulated with phorbol 12-myristate 13-acetate (PMA; Sigma-Aldrich), ionomycin (Sigma-Aldrich), and GolgiStop (BD Biosciences, San Jose, CA, USA) for 5 h. To prevent nonspecific Fc receptor-mediated binding, cells were incubated with anti-CD32 antibody (BD Biosciences) for 10 min and subsequently stained with the appropriate surface antibodies for 30 min at 4 °C (Table S4). Cells were then fixed and permeabilized, followed by intracellular staining for IFN-γ and IL-17A using the corresponding antibodies (Table S4). After staining, cells were washed with staining buffer consisting of PBS supplemented with 1% FBS and analyzed by flow cytometry. $CD4^+$ T-cell populations were identified using sequential gating based on

forward scatter (FSC) and side scatter (SSC), followed by CD4 and intracellular cytokine expression, with 5 × 10^4 events collected per sample. Appropriate fluorescence-minus-one (FMO) and isotype controls were used to establish gating boundaries and ensure accurate population identification. Data were acquired using a FACSCalibur flow cytometer (BD Biosciences) and analyzed using CellQuest Pro software (BD Biosciences).

BV2 and bEnd.3 cell culture and naltrexone treatment

Mouse BV2 microglial cells and mouse brain microvascular endothelial bEnd.3 cells were cultured in Dulbecco's modified Eagle medium (DMEM) supplemented with 10% FBS and 1% penicillin–streptomycin at 37 °C in a humidified atmosphere containing 5% CO_2. Cells were seeded in culture plates and allowed to attach for 24 h before treatment. Prior to the mechanistic experiments, the effects of NTX on cell viability were assessed by MTT assay over a range of concentrations in both BV2 and bEnd.3 cells. The NTX concentrations used in subsequent experiments were selected based on these preliminary cell-viability assessments (Supplementary Figure S7A–B). For BV2 experiments, cells were pretreated with naltrexone (NTX; 2, 20, or 200 μM) for 1 h and then stimulated with lipopolysaccharide (LPS; 1 μg/mL) for 4 h. For bEnd.3 experiments, cells were pretreated with NTX (0.01, 0.1, or 1 mM) for 1 h and then stimulated with LPS (5 μg/mL) for 12 h. To further investigate the involvement of TLR4 signaling, parallel experiments were performed using the TLR4 inhibitor TAK-242. BV2 cells were pretreated with NTX (200 μM) or TAK-242 (500 nM) for 1 h before stimulation with LPS (1 μg/mL) for 4 h, whereas bEnd.3 cells were pretreated with NTX (1 mM) or TAK-242 (1 μg/mL) for 1 h before stimulation with LPS (5 μg/mL) for 12 h. Following LPS stimulation, cells were harvested for Western blot analysis. In BV2 cells, Iba-1 and TLR4-mediated inflammatory signaling molecules, including NF-κB, ERK, JNK, and p38 MAPKs and their phosphorylated forms, were analyzed. In bEnd.3 cells, PECAM-1 and the corresponding TLR4-mediated signaling molecules were examined. All in vitro experiments were independently repeated at least three times.

Statistical analysis

Statistical analyses were performed using GraphPad Prism version 10.4.1 (GraphPad Software, San Diego, CA, USA). Data are presented as mean ± SEM. Multiple-group comparisons were performed using one-way ANOVA with Dunnett's post hoc test, while time-course data were analyzed using two-way repeated-measures ANOVA with Dunnett's post hoc test. Histological scores were evaluated using the Kruskal–Wallis test with Dunn's post hoc test. A P value < 0.05 was considered statistically significant. *In vitro* experiments were independently repeated at least three times unless otherwise indicated.

Results

Characterization of naltrexone-loaded microspheres (IVL4002)

The manufacturing process, morphology, particle size distribution, and physicochemical properties of naltrexone-loaded PLGA microspheres (IVL4002) were characterized using process schematics, SEM, laser diffraction analysis, and formulation analysis (Figure 1, Table S5). IVL4002 was manufactured using the IVL-DrugFluidic® microfluidic platform, in which the aqueous phase and oil phase containing PLGA and naltrexone were delivered by precision pumps into a multi-channel microfluidic processor to generate monodisperse droplets, followed by solvent extraction, washing, and drying (Figure 1A). SEM images showed that the resulting microspheres were uniformly spherical with smooth surfaces, without apparent structural collapse or visible surface pores (Figure 1B). These morphological characteristics were consistent with the controlled droplet generation achieved by the microfluidic manufacturing process.

Laser diffraction analysis revealed a narrow particle size distribution (Figure 1C), with D10, D50, and D90 values of 47.35, 54.88, and 61.58 μm, respectively, and a mean particle diameter of 54.88 μm (Table S5). The coefficient of variation (CV) was 10.41%, and the Span value was 0.26, further indicating a relatively uniform particle size distribution. In addition, IVL4002 exhibited an encapsulation efficiency of 88.97% and a residual solvent level of 11 ppm (Table S5), indicating efficient naltrexone encapsulation and well-controlled physicochemical characteristics of the formulation.

Pharmacokinetics of IVL4002 following a single subcutaneous injection in mice

IVL4002 was designed as a long-acting injectable (LAI) formulation to provide prolonged systemic exposure to naltrexone following a single administration (Figure 2A). Following a single subcutaneous injection of IVL4002 at 0.2, 1, or 10 mg/head, plasma naltrexone concentrations were monitored for 35 days (Figs. 2B and 2C). Systemic exposure increased with increasing dose, with peak plasma concentrations (Cmax) values of 0.73, 3.19, and 31.74 ng/mL and corresponding AUClast values of

296.62, 1,164.10, and 15,649.18 h·ng/mL for the 0.2, 1, and 10 mg groups, respectively (Table 1). The corresponding average plasma concentrations (Cavg) over the 35-day observation period were 0.35, 1.39, and 18.63 ng/mL. Tmax was 504 h in the 0.2 and 10 mg groups and 24 h in the 1 mg group. Collectively, these findings demonstrate prolonged systemic exposure to naltrexone following a single administration of IVL4002, with greater overall exposure at increasing doses, supporting the intended long-acting pharmacokinetic profile of the formulation.

Table 1. Pharmacokinetic parameters following a single-dose pharmacokinetic study of IVL4002 in mice.

Dose (mg/head)	Dosing regimen	Tmax (h)	Cmax (ng/ml)	Cmin (ng/ml)	AUClast (ng·h/ml)	Cavg (ng/ml)
0.2		504.0	0.73	0.00	296.62	0.35
1	Single SC injection	24.0	3.19	0.16	1164.10	1.39
10		504.0	31.74	1.51	15649.18	18.63

Footnote: SC, subcutaneous; Tmax, time to maximum plasma concentration; Cmax, maximum plasma concentration; Cmin, minimum plasma concentration; AUClast, area under the plasma concentration–time curve to the last measurable concentration; Cavg, average plasma concentration.

Safety of IVL4002

During the study period, no IVL4002-related abnormalities in body weight or food consumption were observed in either the low- or high-dose groups in rats or dogs compared with the vehicle or placebo control groups (Table S6). Clinical pathology parameters also revealed no adverse or clinically meaningful changes in any treatment group. Histopathological examination of major organs revealed no IVL4002-related findings in either species (Table 2). The only notable observation was limited to the injection site. At the injection site, granulomatous inflammation characterized by mononuclear cell infiltration and multinucleated giant cell formation was observed in both the placebo and IVL4002-treated groups. These findings were considered a local reaction associated with microsphere administration rather than a compound-related toxic effect. Such granulomatous responses are well-recognized foreign-body reactions commonly observed following implantation of biodegradable microspheres. Overall, repeated administration of IVL4002 produced no evidence of systemic toxicity and was well tolerated in

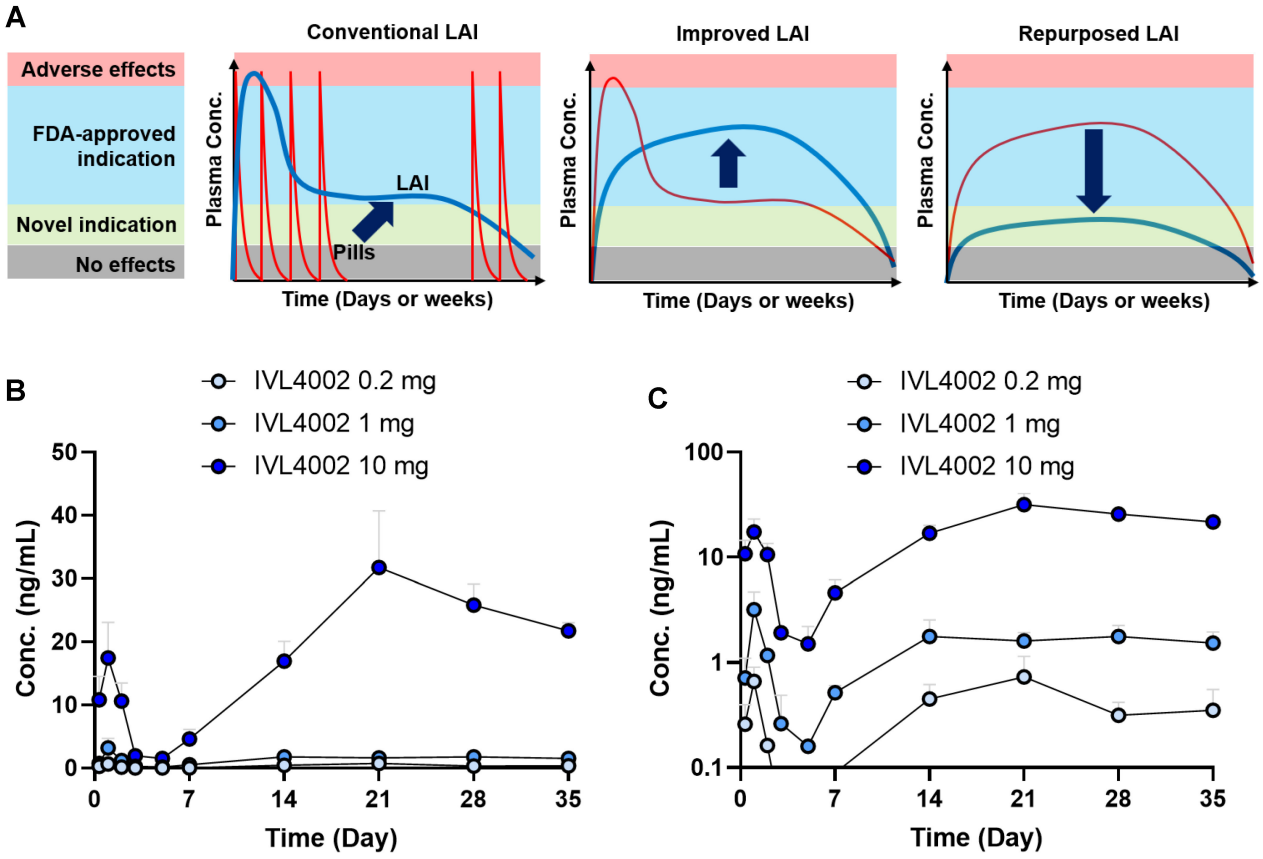


Figure 2. Pharmacokinetic profile of IVL4002 following a single subcutaneous administration in mice. (A) Conceptual schematic illustrating conventional and improved long-acting injectable (LAI) pharmacokinetic profiles and the repurposing strategy enabled by sustained drug exposure. Conventional oral dosing produces repeated peak plasma concentrations, whereas conventional LAI formulations may generate a high initial peak followed by a gradual decline. Improved LAI formulations are designed to reduce excessive peak exposure while maintaining plasma drug concentrations within a therapeutic window over an extended period. The repurposed LAI strategy illustrates the concept of utilizing controlled, sustained exposure at lower plasma concentrations for therapeutic application in a novel indication. **(B, C)** Plasma naltrexone concentration–time profiles following a single subcutaneous administration of IVL4002 at 0.2, 1, or 10 mg/head in mice, presented on linear (B) and logarithmic (C) scales.

both rats and dogs. Histopathological examination of the injection sites demonstrated mild granulomatous inflammation in both placebo microsphere- and IVL4002-treated animals in rats and dogs (Figure S1). In the rat study, mild mixed inflammatory cell infiltration with focal hemorrhage was additionally observed in the single-dose IVL4002 group. No severe inflammation, tissue necrosis, or other adverse local pathological changes were detected. Overall, the incidence and severity of the injection-site findings were comparable between placebo and IVL4002 groups, indicating that these changes were consistent with an expected local foreign-body response to biodegradable PLGA microspheres rather than IVL4002-related local toxicity.

Table 2. Injection-site histopathological findings in rat and dog toxicity studies.

A. Histopathological findings at the subcutaneous injection site in rats								
	Male				Female			
Finding	G1	G2	G3	G4	G1	G2	G3	G4
Inflammation, mixed cell	7	0	0	0	10	0	1	0
Hemorrhage	2	5	3	9	2	7	1	7
Granulomatous inflammation	0	10	10	10	0	10	8	10
B. Histopathological findings at the subcutaneous injection site in dogs								
	Male				Female			
Finding	G1	G2	G3	G4	G1	G2	G3	G4
Inflammation, neutrophilic	0	2	0	1	0	1	0	3
Granulomatous inflammation	0	1	1	0	0	1	0	0

Footnote: Data are presented as mean ± SD for body weight or as the number of animals exhibiting the indicated histopathological finding. Rat study: n = 10 animals/sex/group. Dog study: n = 3 animals/sex/group. G1, vehicle control; G2, placebo control; G3, IVL4002 low dose; G4, IVL4002 high dose. Histopathological findings were confined to the subcutaneous injection site.

IVL4002 ameliorates motor dysfunction and spinal cord demyelination in EAE mice

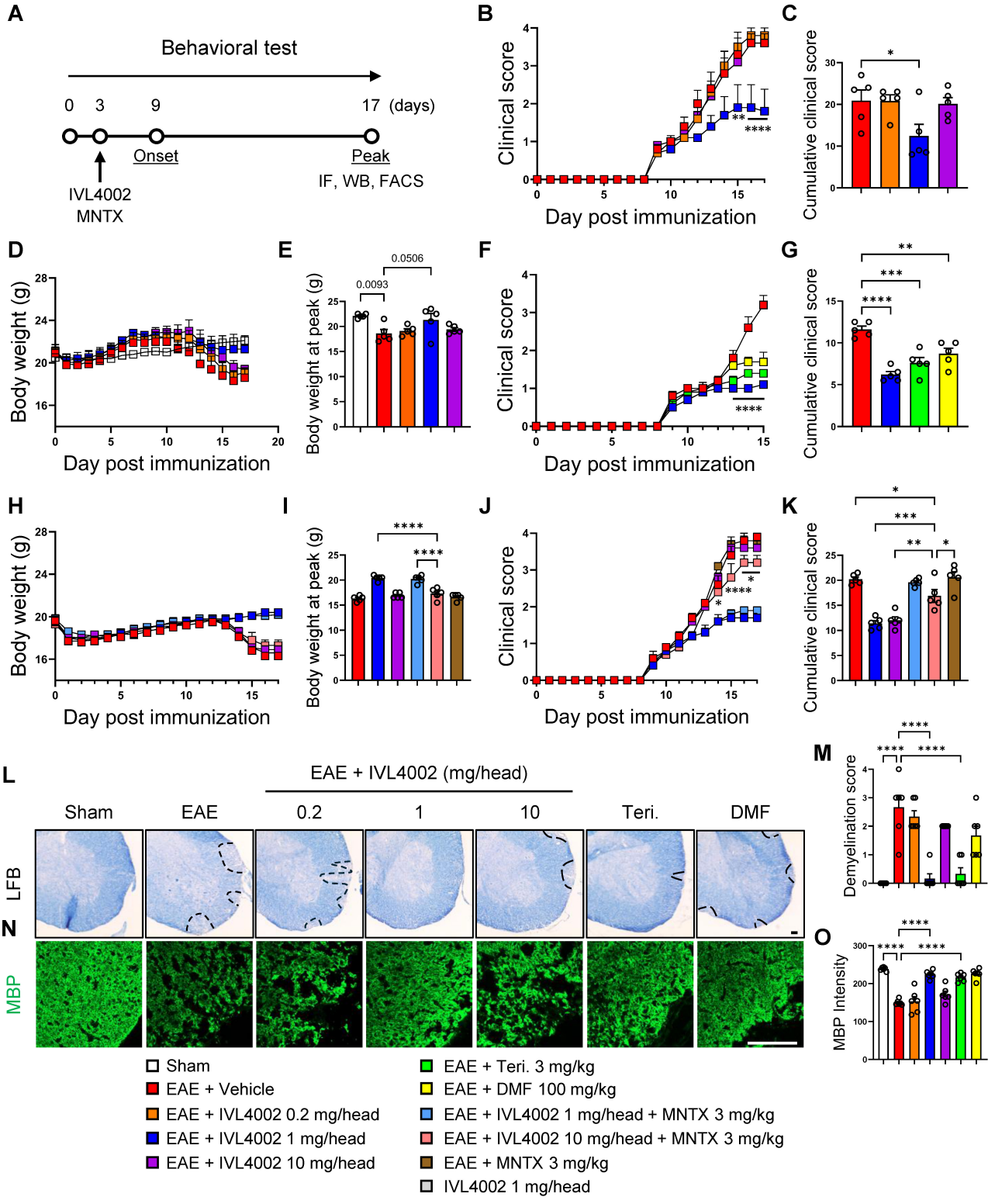
To define the dose range for efficacy evaluation, we first performed a preliminary dose-finding study using IVL4002 at 1, 5, and 10 mg/head. Among the doses tested, 1 mg/head produced the greatest attenuation of EAE clinical severity (Figure S2); therefore, 1 mg/head was selected as the most effective dose among those tested, with 0.2 and 10 mg/head included as lower and higher doses, respectively, for subsequent evaluation.

To evaluate the therapeutic efficacy of IVL4002, we examined whether a single subcutaneous administration of IVL4002 (0.2, 1, or 10 mg/head) at 3 days after immunization could attenuate neurological deficits in EAE mice (Figure 3A). The EAE + vehicle group developed progressive neurological impairment beginning around day 9 after immunization, which progressed to severe hindlimb paralysis at the peak of disease (days 16–17) (Figure 3B). Among the tested doses, IVL4002 administered at 1 mg/head significantly attenuated the progression of neurological deficits compared with the EAE + vehicle group (Figure 3B). Consistently, cumulative clinical scores from days 9 to 17 were markedly reduced in the IVL4002 1 mg/head group compared with the EAE + vehicle group (EAE, 20.9 ± 2.6 vs. EAE + IVL4002 1 mg/head, 12.4 ± 1.5, P = 0.0366) (Figure 3C). In contrast, IVL4002 administered at 0.2 or 10 mg/head did not produce a significant improvement in disease severity. Body weight changes generally reflected disease progression. The EAE + vehicle group exhibited a progressive reduction in body weight during peak disease. At the peak stage, body weight tended to be higher in the IVL4002-treated groups than in the EAE + vehicle group; however, none of these differences reached statistical significance, including the 0.2 mg/head group (P = 0.0506) (Figure 3D–E). Histological examination of the liver revealed no apparent pathological alterations following IVL4002 treatment at any of the doses tested, and liver weights did not differ significantly among the groups (Figure S3A-B). To compare the efficacy of IVL4002 with currently approved disease-modifying therapies for MS, we evaluated its effects alongside those of teriflunomide (3 mg/kg) and DMF (100 mg/kg). IVL4002 at 1 mg/head significantly reduced both daily and cumulative clinical scores, with effects similar to those observed with teriflunomide and DMF (Figure 3F-G).

To further investigate the bell-shaped pattern of therapeutic efficacy observed across IVL4002 doses (Figure 3B-G), MNTX, a peripherally restricted μ-opioid receptor antagonist, was co-administered with IVL4002. Co-treatment with MNTX had little effect on body weight or clinical disease severity in mice receiving IVL4002 at 1 mg/head (Figure 3H-K). In contrast, MNTX partially restored the therapeutic efficacy of IVL4002 at 10 mg/head, resulting in significantly lower clinical scores and cumulative disease severity compared with mice receiving IVL4002 alone at the same dose (Figure 3J-K). These findings suggest that peripheral MOR signaling may contribute, at least in part, to the reduced therapeutic efficacy observed at the higher IVL4002 dose.

To determine whether the therapeutic effects of IVL4002 were accompanied by preservation of lumbar spinal cord myelin, we assessed myelin integrity using histological, immunofluorescence, and Western blot analysis. LFB staining revealed extensive white matter demyelination in the EAE + vehicle group, which was significantly reduced by IVL4002 at 1 mg/head (EAE, 2.67 ± 0.42 vs. EAE + IVL4002 1 mg/head, 0.17 ± 0.17, P < 0.0001), with an effect similar to those observed

with teriflunomide and DMF; no significant protection was observed at 0.2 or 10 mg/head (Figure 3L-M). Consistent with these findings, MBP immunoreactivity was markedly reduced in the EAE + vehicle group but significantly preserved by IVL4002 at 1 mg/head (EAE, 150.10 ± 2.91 vs. EAE + IVL4002 1 mg/head, 224.30 ± 4.32, $P < 0.0001$), whereas the 0.2 and 10 mg/head doses showed no significant effect (Figure 3N-O). Western blot analysis further confirmed significant restoration of spinal cord MBP protein levels by IVL4002 at 1 mg/head (EAE, 108.30 ± 25.58 vs. EAE + IVL4002 1 mg/head, 223.00 ± 25.38, $P = 0.0055$), but not at 0.2 or 10 mg/head (Figure 3P-Q; Figure S4A-B).



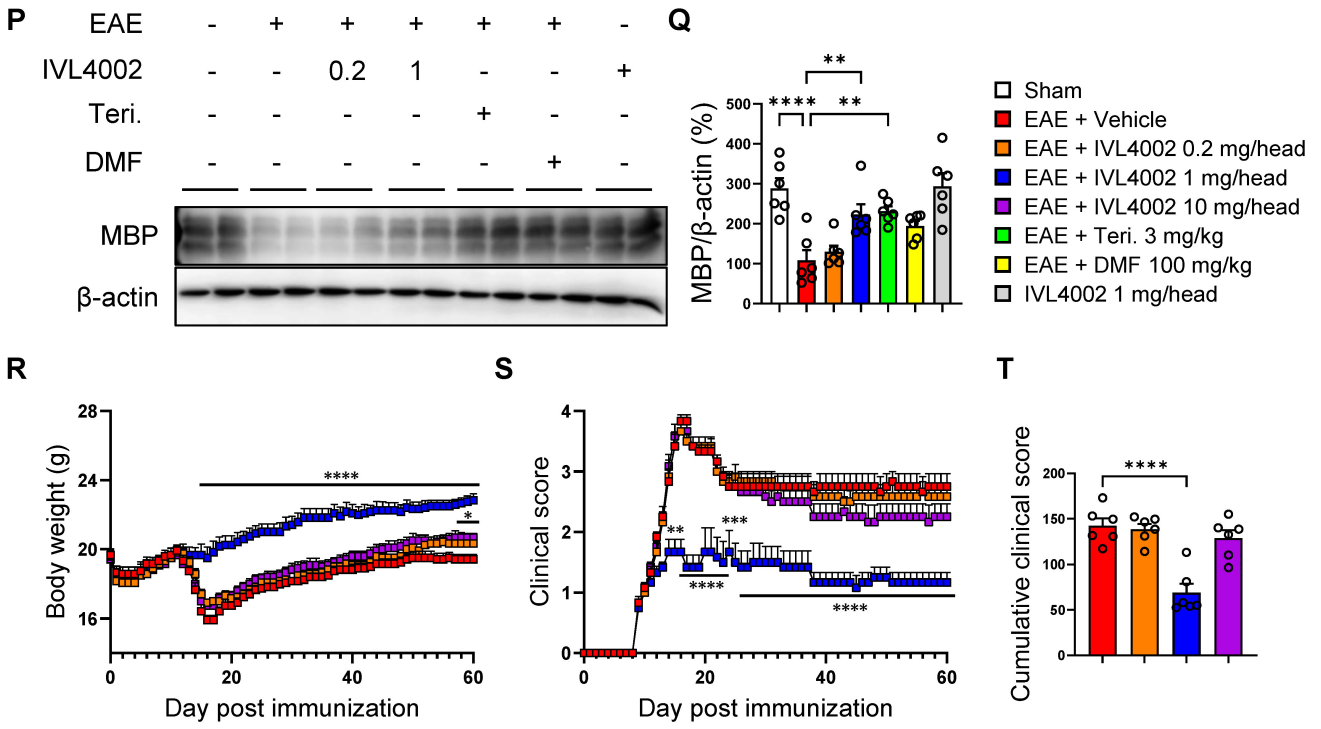


Figure 3. IVL4002 provides sustained therapeutic efficacy and preserves spinal cord myelin in EAE mice. (A–G) Therapeutic efficacy of IVL4002 in EAE mice. **(A)** Experimental design of the acute EAE study. EAE was induced by immunization, and IVL4002 was administered subcutaneously at 3 days after immunization. Behavioral assessments were performed throughout disease progression, and tissues were collected at the peak stage for histological, immunofluorescence, Western blot, and flow cytometric analyses. **(B–E)** Time course of clinical scores (B), cumulative clinical scores from days 9 to 17 post-immunization (C), body weight changes (D), and body weight at the peak stage (E) (n = 5 mice per group). **(F, G)** Comparison of the therapeutic efficacy of IVL4002 with teriflunomide (Teri.; 3 mg/kg) and dimethyl fumarate (DMF; 100 mg/kg): time course of clinical scores (F) and cumulative clinical scores from days 9 to 16 post-immunization (G) (n = 5 mice per group). **(H–K)** Effect of methylnaltrexone (MNTX) co-treatment on the differential therapeutic efficacy of IVL4002 across doses (n = 5 mice per group). **(H, I)** Body weight changes (H) and body weight at the peak stage (I). **(J, K)** Time course of clinical scores (J) and cumulative clinical scores (K). **(L–Q)** Effects of IVL4002 on lumbar spinal cord myelin preservation. **(L, M)** Representative Luxol Fast Blue-stained spinal cord sections at the peak stage of EAE (L) and quantification of demyelination (M). **(N, O)** Representative immunofluorescence images of myelin basic protein (MBP) in spinal cord sections (N) and quantification of MBP fluorescence intensity (O). Scale bar, 50 μm. **(P, Q)** Representative Western blot images showing MBP expression in spinal cord tissue (P) and densitometric quantification of MBP protein levels normalized to β-actin (Q). **(R–T)** Long-term therapeutic efficacy following a single administration of IVL4002. Mice were monitored for 60 days following a single subcutaneous administration of IVL4002 at 3 days after immunization. **(R)** Body weight changes during the 60-day observation period. **(S)** Time course of clinical scores. **(T)** Cumulative clinical scores during the extended observation period. Data are presented as mean ± SEM (n = 6 mice per group). **P* < 0.05, ***P* < 0.01, ****P* < 0.001, and *****P* < 0.0001.

To evaluate the long-term therapeutic efficacy of IVL4002, mice were monitored for up to 60 days after immunization following a single administration at 3 days after immunization (Figure 3R-S). IVL4002 at 1 mg/head resulted in sustained preservation of body weight throughout the 60-day observation period compared with the EAE + vehicle group (Figure 3R). Consistently, IVL4002 at 1 mg/head significantly suppressed clinical disease severity throughout the extended observation period (Figure 3S), and cumulative clinical scores during days 9–60 were significantly reduced (Figure 3T). Collectively, these results demonstrate that IVL4002 effectively attenuates neurological deficits and spinal cord demyelination in EAE mice, with 1 mg/head showing the greatest therapeutic efficacy among the doses tested. Moreover, a single administration of IVL4002 provided durable therapeutic efficacy throughout the 60-day observation period.

IVL4002 suppresses glial activation and neuroinflammation in the spinal cord of EAE mice

Demyelinated lesions in MS and EAE are typically accompanied by pronounced inflammatory cell infiltration [3]. To determine whether IVL4002 modulates inflammatory responses within the spinal cord, H&E staining was performed on lumbar spinal cord (L4–L6) sections collected at peak disease (Figure 4A, upper panel, B). As expected, EAE + vehicle mice exhibited extensive inflammatory cell infiltration throughout the white matter. In contrast, treatment with IVL4002 at 1 mg/head markedly reduced inflammatory infiltration (EAE, 4.67 ± 0.21 vs. EAE + IVL4002 1 mg/head, 2.17 ± 0.40, $P = 0.0013$), whereas the 0.2 and 10 mg/head doses produced minimal effects. To further characterize the inflammatory cell populations affected by IVL4002, immunofluorescence staining for Iba-1 was performed to assess microglial activation and infiltration of microglial/macrophages. Iba-1 immunoreactivity was markedly increased in the

lumbar spinal cords of EAE + vehicle mice compared with sham controls. Notably, IVL4002 treatment at 1 mg/head significantly suppressed this increase (EAE, 66.54 ± 2.39 vs. EAE + IVL4002 1 mg/head, 25.94 ± 6.61, P = 0.038), whereas the 0.2 and 10 mg/head doses failed to produce significant inhibition (Figure 4A, middle panel, C). Because astrocytes are key regulators of neuroinflammatory responses in MS and EAE lesions, astrocytic activation was next evaluated using GFAP immunofluorescence staining [30]. GFAP immunoreactivity was strongly elevated in EAE + vehicle mice compared with sham controls. Importantly, treatment with IVL4002 at 1 mg/head significantly reduced GFAP expression (EAE, 36.63 ± 3.95 vs. EAE + IVL4002 1 mg/head, 8.53 ± 1.28, P < 0.0001), reaching levels comparable to those observed in mice treated with the disease-modifying drugs teriflunomide (3 mg/kg) and DMF (100 mg/kg). In contrast, IVL4002 at 0.2 or 10 mg/head had little effect on astrocytic activation (Figure 4A, lower panel, D).

Consistent with the H&E staining and immunofluorescence findings, Western blot analysis of lumbar spinal cord tissue confirmed that protein levels of Iba-1 and GFAP were markedly elevated in EAE + vehicle mice and were significantly reduced by IVL4002 treatment at 1 mg/head [Iba-1 (EAE, 224.50 ± 22.75 vs. EAE + IVL4002 1 mg/head, 126.90 ± 17.47, P = 0.0055), GFAP (EAE, 218.70 ± 23.77 vs. EAE + IVL4002, 117.60 ± 7.19, P = 0.0021)], whereas minimal changes were observed at the lower or higher doses (Figure 4E-G). In contrast, IVL4002 at 10 mg/head did not significantly attenuate the EAE-induced increases in Iba-1 and GFAP expression (Figure S4A, C, D). To determine whether suppression of glial activation by IVL4002 was associated with modulation of inflammatory signaling, quantitative RT-PCR analysis was performed on spinal cord tissue. The mRNA expression of representative inflammatory mediators, including *Nos2*, *Il6*, *Ccl2*, and *Ccl3*, was markedly increased in EAE + vehicle mice compared with sham controls and was significantly attenuated by IVL4002 treatment at 1 mg/head, whereas the 0.2 mg/head dose exerted minimal effects (Figure 4H–K; Figure S4E).

Collectively, these findings demonstrate that IVL4002 suppresses neuroinflammatory responses in the spinal cord of EAE mice by inhibiting microglial activation, monocyte-derived macrophage infiltration, and astrocytic activation, accompanied by reduced expression of inflammatory mediators. These results indicate that the therapeutic effects of IVL4002 observed in EAE are closely associated with attenuation of glial-mediated neuroinflammation within demyelinated lesions.

IVL4002 suppresses lymphoid organ hypertrophy, pathogenic CD4⁺ Th1/Th17 cell expansion, and spinal cord T-cell infiltration in EAE mice

Secondary lymphoid organs, including the spleen and lymph nodes, undergo marked hypertrophy during EAE as a consequence of aberrant immune activation [23, 31, 32]. To determine whether IVL4002 modulates this response, spleen and lymph node weights were measured at peak disease (days 16–17 post-immunization) (Figure 5A-C). As expected, the EAE + vehicle group exhibited significant enlargement of both organs compared with sham controls. Notably, IVL4002 at 1 mg/head significantly reduced spleen and lymph node weights, whereas IVL4002 administration to sham mice did not significantly alter either organ weight.

Because expansion of autoreactive CD4⁺ T-cell subsets is a key driver of EAE pathology, we next examined whether IVL4002 alters T-cell populations in secondary lymphoid organs. Flow cytometric analysis of spleen and lymph node cells showed increased proportions of CD4⁺ T cells, pathogenic Th1 (CD4⁺IFN-γ⁺) and Th17 (CD4⁺IL-17A⁺) cells in the EAE + vehicle compared with sham controls (Figure 5D-F, H-J). IVL4002 at 1 mg/head significantly reduced the overall CD4⁺ T-cell population as well as pathogenic Th1 and Th17 cell populations in both the spleen and lymph nodes [CD4⁺/IFN-γ⁺, Spleen (EAE, 10.00 ± 0.73 vs. EAE + IVL4002 1 mg/head, 5.47 ± 1.30, P = 0.0103), Lymph node (EAE, 10.03 ± 1.20 vs. EAE + IVL4002 1 mg/head, 4.02 ± 1.72, P = 0.005)], [CD4⁺/IL-17A ⁺, Spleen (EAE, 24.85 ± 3.57 vs. EAE + IVL4002 1 mg/head, 14.59 ± 2.83, P = 0.0359), Lymph node (EAE, 32.08 ± 1.01 vs. EAE + IVL4002 1 mg/head, 25.38 ± 1.43, P = 0.0284)]. In contrast, IVL4002 administration to sham mice did not significantly alter basal T-cell populations. CD8⁺ T-cell populations were not significantly altered by IVL4002 treatment (Figure 5G-K). Because pathogenic autoreactive T cells generated in peripheral lymphoid organs subsequently migrate into the CNS and contribute to demyelinating pathology, we next evaluated T-cell infiltration into the spinal cord. Flow cytometric analysis revealed marked increases in CD4⁺ T cells, pathogenic Th1 (CD4⁺IFN-γ⁺) and Th17 (CD4⁺IL-17A⁺) cells in the lumbar spinal cord of the EAE + vehicle group compared with sham controls. IVL4002 at 1 mg/head significantly reduced the infiltration of these CD4⁺ T-cell populations into the spinal cord (Figure 5L-N). In contrast, CD8⁺ T-cell infiltration was not significantly affected by IVL4002 treatment (Figure 5O). Representative gating strategies and flow cytometric profiles for T-cell subset analysis in the spleen, draining lymph nodes, and lumbar spinal cord are shown in Figure S5.

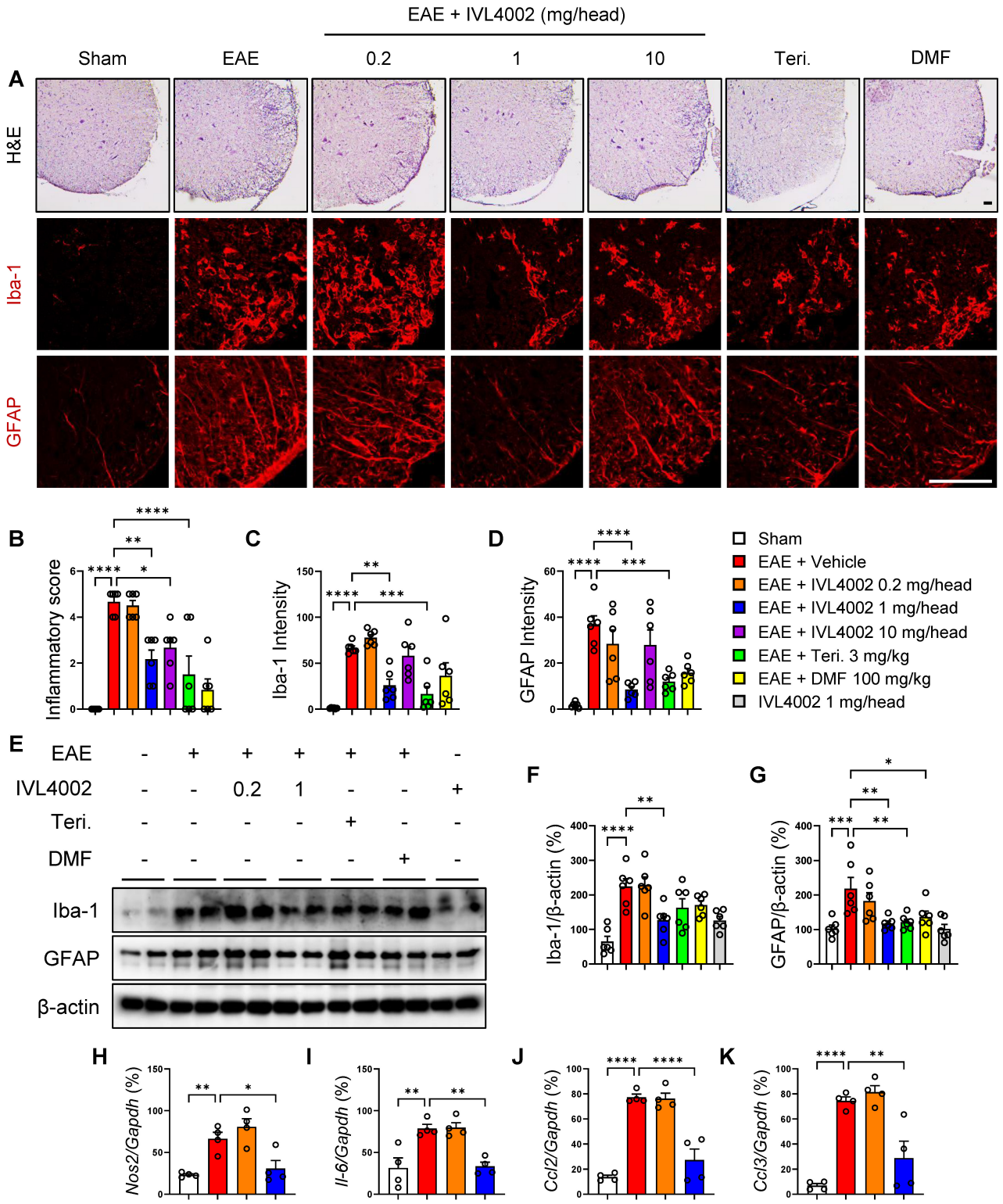


Figure 4. IVL4002 suppresses neuroinflammation and glial activation in the spinal cord of EAE mice. (A) Representative H&E-stained sections and immunofluorescence images of Iba-1 and GFAP in the lumbar spinal cord from sham, EAE + vehicle, and EAE mice treated with IVL4002 (0.2, 1, or 10 mg/head), Teri. (3 mg/kg), or DMF (100 mg/kg). **(B)** Semi-quantitative inflammatory scores derived from H&E-stained spinal cord sections. **(C, D)** Quantification of Iba-1 (C) and GFAP (D) fluorescence intensity. Scale bars, 50 μm. **(E–G)** Western blot analysis of Iba-1 and GFAP expression in spinal cord tissue. **(E)** Representative Western blot images of Iba-1 and GFAP, with β-actin used as a loading control. **(F, G)** Densitometric quantification of Iba-1 (F) and GFAP (G) protein levels normalized to β-actin. **(H–K)** Semi-quantitative RT-PCR analysis of inflammatory mediator expression in spinal cord tissue, including *Nos2* (H), *Il6* (I), *Ccl2* (J), and *Ccl3* (K). Expression levels were normalized to *Gapdh*. Representative RT-PCR bands are shown in Figure S4E. Data are presented as mean ± SEM (n = 6 per group). **P* < 0.05, ***P* < 0.01, ****P* < 0.001, and *****P* < 0.0001.

To further validate the flow cytometric findings and provide spatial evidence of pathogenic T-cell infiltration within the spinal cord, we performed immunofluorescence staining of lumbar spinal cord

sections for CD4 and IFN-γ or CD4 and IL-17A (Figure 5P-R). Consistent with the flow cytometric analyses, the EAE + vehicle group exhibited marked accumulation of $CD4^+IFN\text{-}\gamma^+$ (Th1) and $CD4^+IL\text{-}17A^+$ (Th17) cells in the spinal cord, which was markedly reduced by IVL4002 treatment [$CD4^+/IFN\text{-}\gamma^+$ (EAE, 18.24 ± 1.34 vs. EAE + IVL4002 1 mg/head, 11.09 ± 2.28, $P = 0.0065$)], [$CD4^+/IL\text{-}17A^+$ (EAE, 22.95 ± 0.20 vs. EAE + IVL4002 1 mg/head, 16.97 ± 1.98, $P = 0.0031$)] (Figure 5P, Figure S6). Quantitative analysis further confirmed significant reductions in $CD4^+IFN\text{-}\gamma^+$ and $CD4^+IL\text{-}17A^+$ fluorescence intensities in IVL4002-treated mice compared with the EAE + vehicle group [$CD4^+/IFN\text{-}\gamma^+$ (EAE, 12.82 ± 2.61 vs. EAE + IVL4002 1 mg/head, 2.93 ± 1.16, $P = 0.0008$)], [$CD4^+/IL\text{-}17A^+$ (EAE, 9.87 ± 2.37 vs. EAE + IVL4002 1 mg/head, 1.92 ± 0.37, $P = 0.0008$)] (Figure 5Q-R).

Collectively, these results demonstrate that IVL4002 suppresses lymphoid organ hypertrophy, limits the expansion of pathogenic $CD4^+$ Th1 and Th17 cells in peripheral lymphoid tissues, and reduces their infiltration into the spinal cord, as supported by both flow cytometric and immunofluorescence analyses.

IVL4002 inhibits TLR4/MyD88/NF-κB/MAPK signaling in the spinal cord of EAE mice

Activation of TLR4-associated inflammatory signaling contributes to the pathogenesis of MS and EAE through downstream NF-κB and MAPK pathways [33-35]. We therefore investigated whether IVL4002 modulates TLR4-associated inflammatory signaling in the lumbar spinal cord of EAE mice by Western blot analysis (Figure 6). TLR4 and MyD88 protein levels were significantly increased in the EAE + vehicle group compared with sham controls. IVL4002 treatment significantly reduced TLR4 expression, with the most pronounced effect observed at 1 mg/head [TLR4 (EAE, 501.80 ± 92.70 vs. EAE + IVL4002 1 mg/head, 293.40 ± 20.23, $P = 0.0341$)], whereas the reduction in MyD88 expression did not reach statistical significance (Figure 6A-C). Consistent with these findings, the phosphorylation of NF-κB p65 was markedly increased in the EAE + vehicle group and significantly attenuated by IVL4002, with 1 mg/head [NF-κB p65/NF-κB (EAE, 160.90 ± 20.08 vs. EAE + IVL4002 1 mg/head, 48.03 ± 8.52, $P = 0.0008$)] showing the strongest inhibitory effect among the doses tested (Figure 6A, D). Similarly, phosphorylation of the MAPKs ERK, JNK, and p38 was markedly elevated in the EAE + vehicle group and significantly attenuated by IVL4002 treatment [p-ERK/ERK (EAE, 163.60 ± 16.72 vs. EAE + IVL4002 1 mg/head, 85.62 ± 12.07, $P = 0.0004$)], [p-JNK/JNK (EAE, 163.70 ± 19.27 vs. EAE + IVL4002 1 mg/head, 105.80 ± 13.27, $P = 0.0068$)], [p-p38/p38 (EAE, 192.40 ± 9.47 vs. EAE + IVL4002 1 mg/head, 81.60 ± 9.78, $P < 0.0001$)] (Figure 6A, E-G). Overall, IVL4002 at 1 mg/head produced the most consistent suppression across the TLR4/MyD88/NF-κB/MAPK signaling components examined. The effects observed with IVL4002 were generally similar to those observed with teriflunomide (3 mg/kg) and DMF (100 mg/kg), whereas IVL4002 administration to sham mice did not significantly alter these signaling molecules.

Collectively, these results indicate that IVL4002 attenuates TLR4/MyD88-associated NF-κB and MAPK signaling in the spinal cord, with the most consistent effects observed at 1 mg/head among the doses tested, supporting suppression of inflammatory signaling as a potential mechanism underlying its therapeutic effects in EAE.

Naltrexone suppresses TLR4-associated NF-κB/MAPK signaling in LPS-stimulated microglia

Because IVL4002 suppressed microglial activation (Figure 4) and attenuated TLR4-associated NF-κB/MAPK signaling in the lumbar spinal cord of EAE mice (Figure 6), we next examined whether naltrexone, the active component of IVL4002, modulates these inflammatory responses in microglia. Preliminary MTT assays showed that naltrexone at concentrations up to 200 μM did not significantly affect BV2 cell viability (Figure S7A). BV2 microglial cells were stimulated with LPS in the presence or absence of naltrexone (2, 20, or 200 μM), followed by Western blot analysis (Figure 7A-I). LPS stimulation markedly increased Iba-1 and iNOS expression, whereas naltrexone treatment attenuated these increases [Iba-1 (LPS, 258.20 ± 18.66 vs. LPS + NTX 200 μM, 105.00 ± 16.38, $P = 0.0006$)], [iNOS (LPS, 376.10 ± 22.95 vs. LPS + NTX 200 μM, 116.00 ± 11.90, $P < 0.0001$)] (Figure 7B-D). Similarly, LPS-induced TLR4 expression and NF-κB p65 phosphorylation were significantly reduced by naltrexone [TLR4 (LPS, 175.00 ± 41.81 vs. LPS + NTX 200 μM, 72.40 ± 10.10, $P = 0.0421$)], [NF-κB p65/NF-κB (LPS, 383.70 ± 19.51 vs. LPS + NTX 200 μM, 181.60 ± 35.93, $P < 0.0001$)] (Figure 7B, E, F). Naltrexone also attenuated LPS-induced phosphorylation of ERK, JNK, and p38 MAPKs [p-ERK/ERK (LPS, 145.70 ± 5.61 vs. LPS + NTX 200 μM, 71.93 ± 7.85, $P < 0.0001$)], [p-JNK/JNK (LPS, 168.30 ± 19.29 vs. LPS + NTX 200 μM, 59.79 ± 7.89, $P = 0.0011$)], [p-p38/p38 (LPS, 221.50 ± 43.35 vs. LPS + NTX 200 μM, 113.30 ± 9.60, $P = 0.0143$)] (Figure 7B, G-I). In contrast, naltrexone treatment alone (200 μM) did not significantly alter the basal levels of the proteins examined.

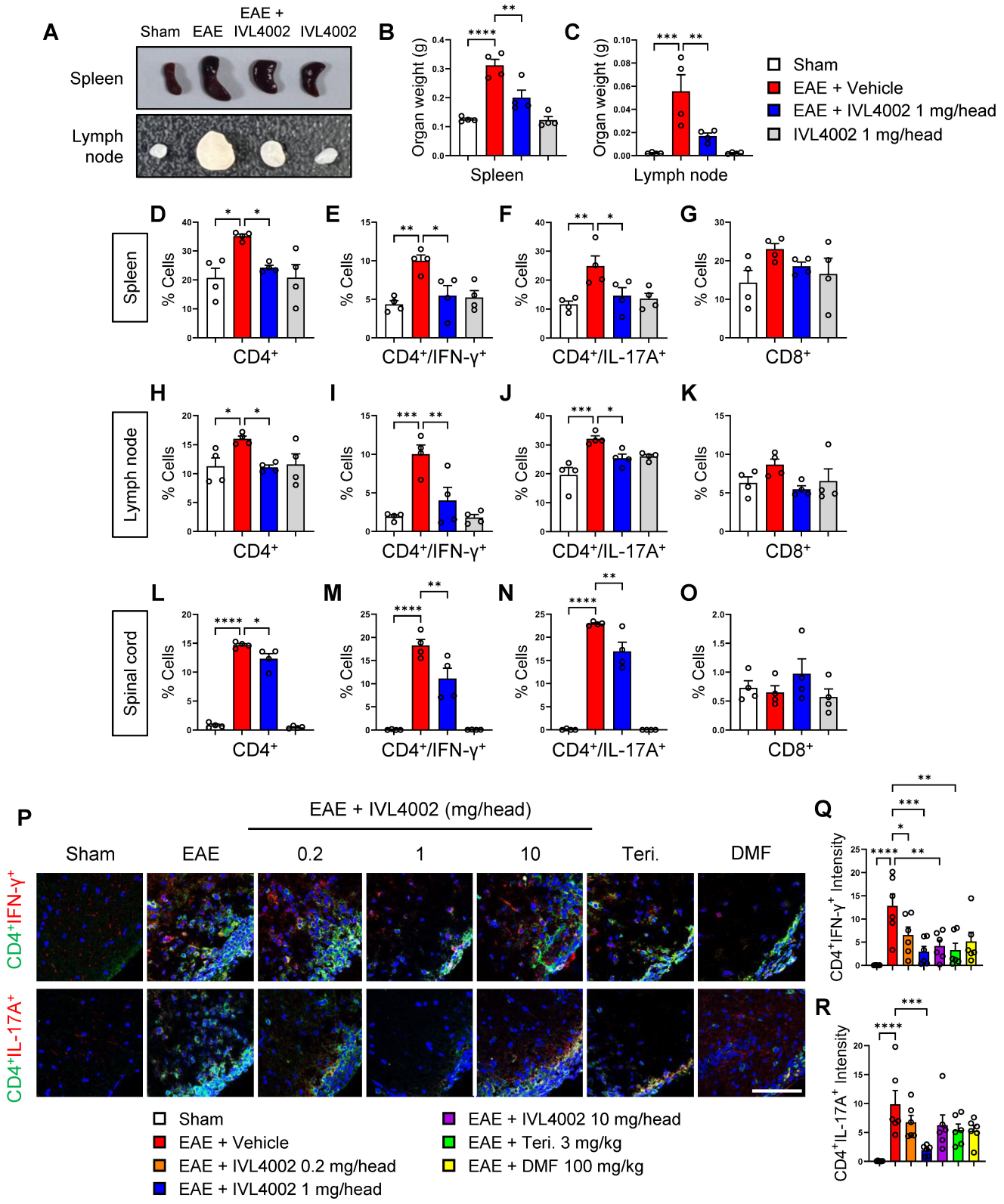


Figure 5. IVL4002 Suppresses lymphoid organ hypertrophy and pathogenic CD4⁺ T-cell responses in EAE mice. (A) Representative gross images of the spleen and draining lymph nodes from sham, EAE + vehicle, EAE + IVL4002, and IVL4002-only mice at the peak stage of disease. **(B, C)** Quantification of spleen (B) and lymph node (C) weights. **(D–G)** Flow cytometric quantification of $CD4^+$ T cells (D), $CD4^+$ IFN-γ⁺ Th1 cells (E), $CD4^+$ IL-17A⁺ Th17 cells (F), and $CD8^+$ T cells (G) in the spleen. **(H–K)** Flow cytometric analysis of $CD4^+$ T cells (H), $CD4^+$ IFN-γ⁺ Th1 cells (I), $CD4^+$ IL-17A⁺ Th17 cells (J), and $CD8^+$ T cells (K) in the draining lymph nodes. **(L–O)** Quantification of $CD4^+$ T cells (L), $CD4^+$IFN-γ⁺ Th1 cells (M), $CD4^+$IL-17A⁺ Th17 cells (N), and $CD8^+$ T cells (O) in the spinal cord. **(P–R)** Immunofluorescence analysis of infiltrating Th1 and Th17 cells in spinal cord sections. **(P)** Representative merged immunofluorescence images of CD4 (green) with IFN-γ (red) or IL-17A (red), with DAPI nuclear counterstaining (blue), showing infiltrating $CD4^+$IFN-γ⁺ Th1 and $CD4^+$IL-17A⁺ Th17 cells, respectively. The corresponding single-channel images are provided in Figure S6. **(Q, R)** Quantification of $CD4^+$IFN-γ⁺ Th1 cells (Q) and $CD4^+$IL-17A⁺ Th17 cells (R). IVL4002 treatment significantly reduced the infiltration of both Th1 and Th17 cells into the spinal cord compared with the EAE + vehicle group. Scale bar, 50 μm. Data are presented as mean ± SEM (n = 4–6 per group). *P < 0.05, **P < 0.01, ***P < 0.001, and ****P < 0.0001.

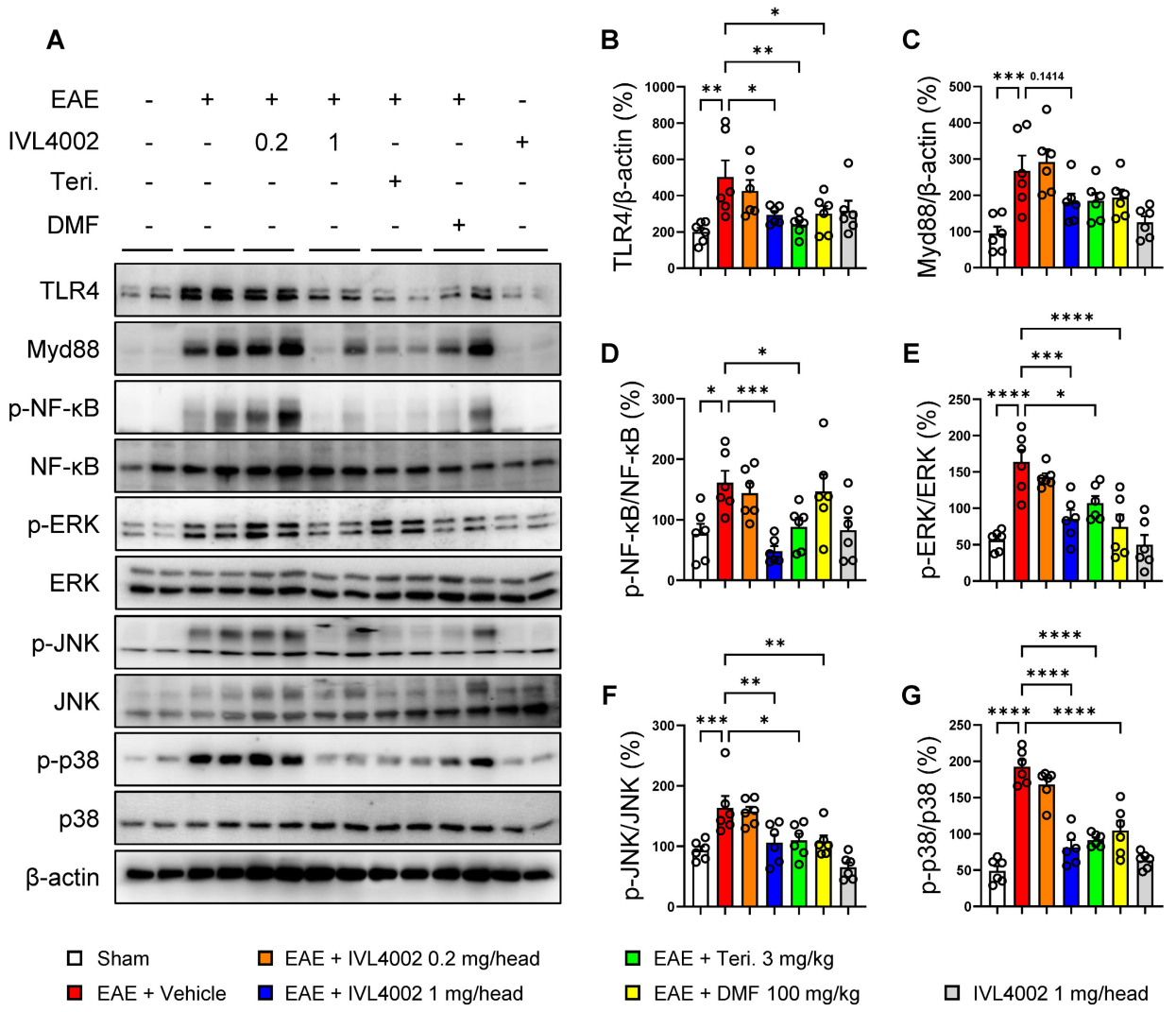


Figure 6. IVL4002 suppresses TLR4/MyD88-associated NF-κB/MAPK signaling in the spinal cord of EAE mice. (A) Representative Western blot images of TLR4, MyD88, NF-κB p65, and MAPK signaling proteins in lumbar spinal cord tissues from sham, EAE + vehicle, and EAE mice treated with IVL4002 (0.2, 1, or 10 mg/head), Teri. (3 mg/kg), or DMF (100 mg/kg), as well as mice treated with IVL4002 alone. Phosphorylated and total forms of NF-κB p65, ERK, JNK, and p38 are shown. β-Actin was used as a loading control. **(B, C)** Densitometric quantification of TLR4 (B) and MyD88 (C) protein levels normalized to β-actin. **(D–G)** Densitometric quantification of the phosphorylation ratios of NF-κB p65 (D), ERK (E), JNK (F), and p38 (G), normalized to their corresponding total protein levels. Data are presented as mean ± SEM (n = 6 mice per group). **P* < 0.05, ***P* < 0.01, ****P* < 0.001, and *****P* < 0.0001.

To further assess the involvement of TLR4 signaling in the inhibitory effects of naltrexone, we compared its effects with those of TAK-242, a selective TLR4 inhibitor, at a concentration that did not significantly affect BV2 cell viability (Figure S7B; Figure 7J). Both naltrexone and TAK-242 attenuated LPS-induced increases in Iba-1 and TLR4 expression and phosphorylation of NF-κB p65, ERK, JNK, and p38 (Figure 7K-Q). The similar patterns of inhibition observed with naltrexone and TAK-242 provide pharmacological support for the involvement of TLR4-associated signaling in the effects of naltrexone on LPS-induced microglial inflammatory responses.

Collectively, these findings demonstrate that naltrexone suppresses LPS-induced microglial inflammatory responses in association with attenuation of TLR4-associated NF-κB/MAPK signaling, while the TAK-242 experiments provide additional pharmacological support for the involvement of TLR4 signaling.

IVL4002 preserves blood–brain barrier integrity in EAE mice

Disruption of the BBB is a hallmark pathological feature of MS and EAE, facilitating the infiltration of peripheral immune cells into the CNS [36]. To directly evaluate BBB integrity *in vivo*, we first assessed Evans Blue extravasation (Figure 8A-D) and albumin (ALB) leakage (Figure 8E-F), followed by immunofluorescence analyses of the endothelial activation marker PECAM-1 and the tight junction proteins CLDN5, OCLN, and ZO-1 in lumbar spinal cord sections obtained at the peak stage of EAE (Figure 8G-N).

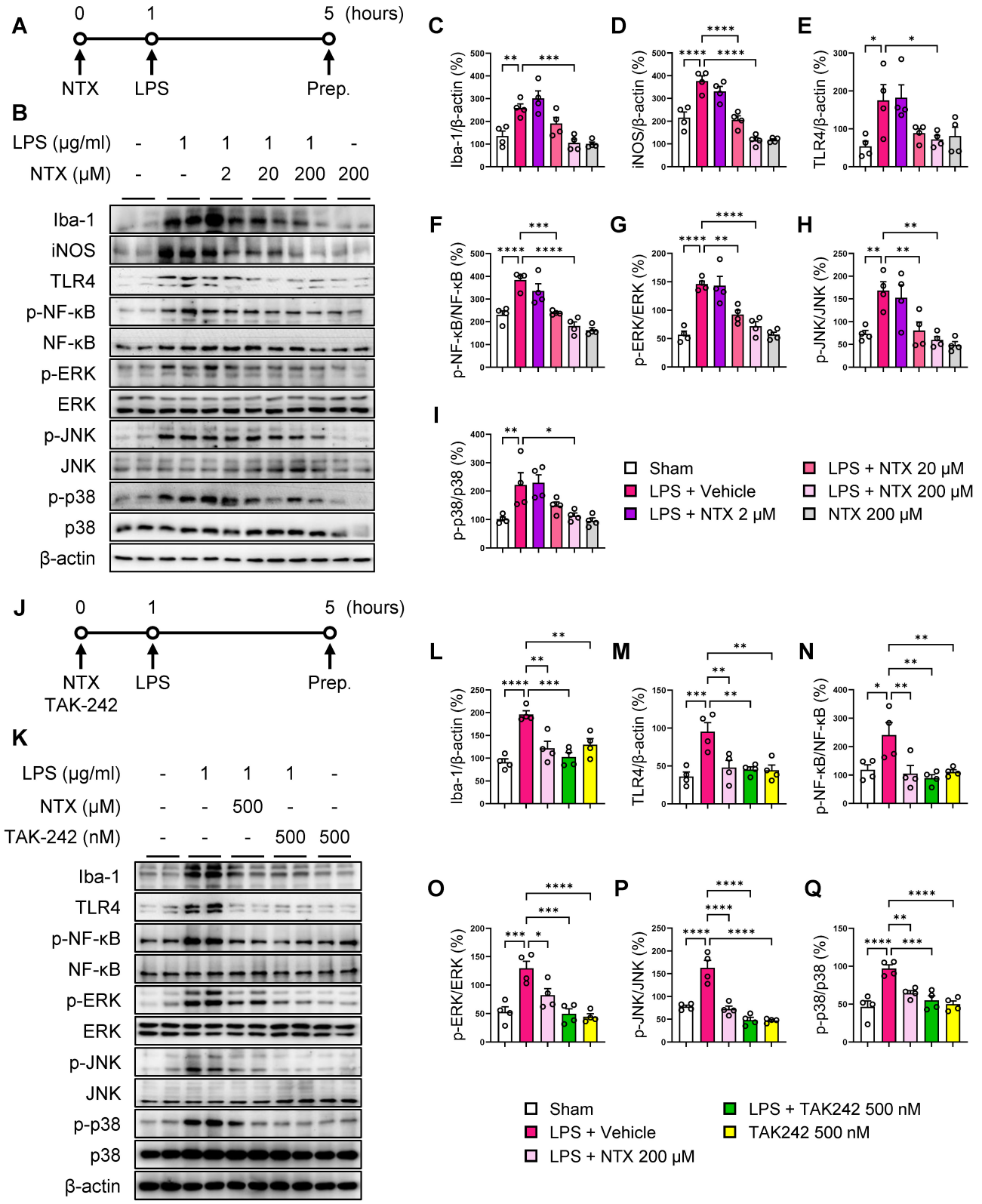


Figure 7. Naltrexone suppresses LPS-induced microglial activation and TLR4-associated NF-κB/MAPK signaling in BV2 cells. (A) Schematic overview of the experimental design. BV2 microglial cells were pretreated with naltrexone (NTX; 2, 20, or 200 μM) for 1 h and subsequently stimulated with lipopolysaccharide (LPS; 1 μg/mL). Cells were harvested 4 h after LPS stimulation for protein analysis. **(B)** Representative Western blot images of Iba-1, inducible nitric oxide synthase (iNOS), TLR4, and phosphorylated and total NF-κB p65, ERK, JNK, and p38. β-Actin was used as a loading control. **(C–E)** Densitometric quantification of Iba-1 (C), iNOS (D), and TLR4 (E) protein levels normalized to β-actin. **(F–I)** Densitometric quantification of the phosphorylation ratios of NF-κB p65 (F), ERK (G), JNK (H), and p38 (I), normalized to their corresponding total protein levels. **(J)** Schematic overview of the experimental design for pharmacological assessment of TLR4 involvement using TAK-242. BV2 cells were pretreated with NTX (200 μM) or TAK-242 (500 nM) for 1 h before LPS stimulation and harvested 5 h later for protein analysis. **(K)** Representative Western blot images of Iba-1, TLR4, and phosphorylated and total NF-κB p65, JNK, ERK, and p38. β-Actin was used as a loading control. **(L, M)** Densitometric quantification of Iba-1 (L) and TLR4 (M) protein levels normalized to β-actin. **(N–Q)** Densitometric quantification of the phosphorylation ratios of NF-κB p65 (N), ERK (O), JNK (P), and p38 (Q), normalized to their corresponding total protein levels. Data are presented as mean ± SEM (n = 4 per group). **P* < 0.05, ***P* < 0.01, ****P* < 0.001, and *****P* < 0.0001.

EAE mice exhibited marked Evans Blue extravasation and ALB leakage into the spinal cord, accompanied by increased PECAM-1 expression and substantial reductions in CLDN5, OCLN, and ZO-1 expression, indicating BBB disruption (Figure 8A-N). In contrast, IVL4002 treatment at 1 mg/head significantly reduced Evans Blue extravasation and ALB leakage while suppressing PECAM-1 expression and preserving the expression of all three tight junction proteins [Evans Blue extravasation (EAE, 4.39 ± 0.22 vs. EAE + IVL4002 1 mg/head, 3.21 ± 0.042, P = 0.0003; vs. EAE + IVL4002 10 mg/head, 3.70 ± 0.14, P = 0.0137); Intensity (EAE, 21.27 ± 4.09 vs. EAE + IVL4002 1 mg/head, 0.03 ± 0.01, P = 0.0002; vs. EAE + IVL4002 10 mg/head, 9.46 ± 2.01, P = 0.0473)], [ALB (EAE, 26.92 ± 5.93 vs. EAE + IVL4002 1 mg/head, 7.06 ± 1.17, P = 0.0041)], [PECAM-1 (EAE, 35.75 ± 5.70 vs. EAE + IVL4002 1 mg/head, 4.83 ± 0.95, P < 0.0001)], [CLDN-5 (EAE, 1.64 ± 0.54 vs. EAE + IVL4002 1 mg/head, 13.70 ± 2.28, P < 0.0001)], [OCLN (EAE, 0.55 ± 0.15 vs. EAE + IVL4002 1 mg/head, 13.40 ± 1.90, P < 0.0001)], [ZO-1 (EAE, 3.19 ± 0.48 vs. EAE + IVL4002 1 mg/head, 21.26 ± 1.08, P < 0.0001)] (Figure 8G-N). Comparable protective effects were observed in the teriflunomide- and DMF-treated groups, whereas the 10 mg/head dose showed only partial protection (Figure 8G-N).

Naltrexone suppresses TLR4-associated NF-κB/MAPK signaling in brain endothelial cells

To further investigate the endothelial mechanisms associated with the effects of IVL4002 on BBB integrity, preliminary MTT assays showed that naltrexone at concentrations up to 1 mM did not significantly affect bEnd.3 cell viability (Figure S7C). Murine brain endothelial bEnd.3 cells were pretreated with naltrexone (0.01, 0.1, or 1 mM) prior to LPS stimulation, followed by Western blot analysis (Figure 9A–H). LPS stimulation markedly increased PECAM-1 and TLR4 expression, both of which were attenuated by naltrexone pretreatment [PECAM-1 (LPS, 160.20 ± 10.49 vs. LPS + NTX 1 mM, 78.16 ± 9.59, P = 0.0002)], [TLR4 (LPS, 132.70 ± 13.00 vs. LPS + NTX 1 mM, 72.19 ± 13.44, P = 0.0454)] (Figure 9B-D). Similarly, LPS-induced phosphorylation of NF-κB p65 was significantly reduced by naltrexone [NF-κB p65/NF-κB (LPS, 215.20 ± 27.30 vs. LPS + NTX 1 mM, 125.40 ± 14.36, P = 0.0063)] (Figure 9B, E). Naltrexone also attenuated LPS-induced phosphorylation of ERK, JNK, and p38 MAPKs [p-ERK/ERK (LPS, 165.60 ± 28.83 vs. LPS + NTX 1 mM, 48.35 ± 2.88, P = 0.0002)], [p-JNK/JNK (LPS, 245.1 ± 60.27 vs. LPS + NTX 1 mM, 92.52 ± 29.13, P = 0.048)], [p-p38/p38 (LPS, 228.50 ± 18.12 vs. LPS + NTX 1 mM, 93.16 ± 14.34, P = 0.0019)] (Figure 9B, F–H). In contrast, naltrexone treatment alone (1 mM) did not significantly alter the basal levels of the proteins examined.

To further assess the involvement of TLR4 signaling in these endothelial inflammatory responses, we compared the effects of naltrexone with those of TAK-242, a selective TLR4 inhibitor, at a concentration that did not significantly affect bEnd.3 cell viability (Figure S7D; Figure 9I). Both naltrexone and TAK-242 attenuated LPS-induced TLR4 expression and phosphorylation of NF-κB p65, ERK, JNK, and p38 (Figure 9J-O). These findings provide pharmacological support for the involvement of TLR4-associated signaling in the inhibitory effects of naltrexone on LPS-induced endothelial inflammatory responses.

Collectively, these findings indicate that naltrexone attenuates LPS-induced inflammatory responses in brain endothelial cells in association with suppression of TLR4-associated NF-κB/MAPK signaling.

Discussion

This study demonstrates that IVL4002, a microfluidic-based sustained-release naltrexone microparticle formulation, exerts significant therapeutic effects in EAE by attenuating neuroinflammation, demyelination, and clinical disease severity. Notably, a single administration at 3 days after immunization produced durable therapeutic efficacy that was maintained throughout the 60-day observation period, highlighting the potential value of controlled-release pharmacology for chronic autoimmune neuroinflammatory conditions. These findings indicate that the therapeutic effects of IVL4002 are associated with coordinated modulation of pathogenic immune responses in peripheral lymphoid tissues and inflammatory processes within the CNS.

Interestingly, therapeutic efficacy in the *in vivo* EAE model varied across the doses tested, with the greatest efficacy observed at 1 mg/head and diminished efficacy at the higher 10 mg/head dose. In contrast, *in vitro* assays demonstrated concentration-dependent suppression of inflammatory signaling as naltrexone concentrations increased. This apparent discrepancy likely reflects differences between simplified *in vitro* systems and the complex physiological environment *in vivo*. We initially hypothesized that, at higher systemic exposure, stronger and more sustained MOR antagonism might engage compensatory inflammatory responses that counterbalance the non-opioid anti-inflammatory effects of naltrexone observed *in vitro* [13, 37, 38].

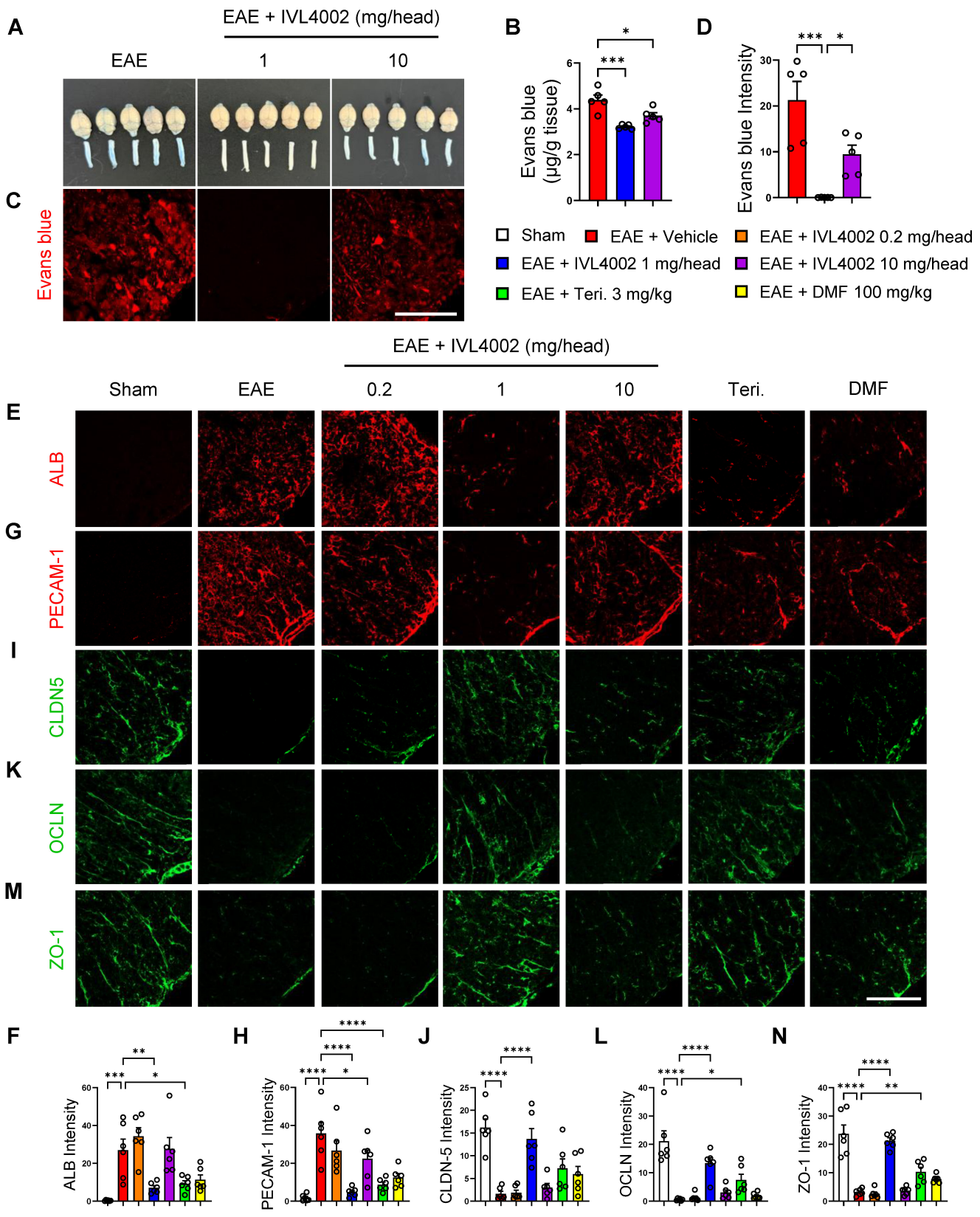


Figure 8. IVL4002 preserves blood–brain barrier integrity in EAE mice. (A–D) Assessment of blood–brain barrier (BBB) integrity by Evans Blue extravasation. **(A)** Representative gross images showing Evans Blue distribution in the brain and lumbar spinal cord. **(B)** Quantification of Evans Blue content in brain tissue. **(C)** Representative fluorescence images of Evans Blue extravasation in spinal cord sections. **(D)** Quantification of Evans Blue fluorescence intensity (n = 5 per group). **(E, F)** Representative immunofluorescence images of albumin (ALB) in spinal cord sections (E) and quantification of ALB fluorescence intensity (F). **(G–N)** Immunofluorescence analysis of the endothelial marker PECAM-1 and the tight junction proteins claudin-5 (CLDN5), occludin (OCLN), and zonula occludens-1 (ZO-1) in spinal cord sections obtained at the peak stage of EAE. Representative images and corresponding quantification of fluorescence intensities are shown for PECAM-1 (G, H), CLDN5 (I, J), OCLN (K, L), and ZO-1 (M, N) (n = 6 per group). Scale bars, 50 μm. Data are presented as mean ± SEM. **P* < 0.05, ***P* < 0.01, ****P* < 0.001, and *****P* < 0.0001.

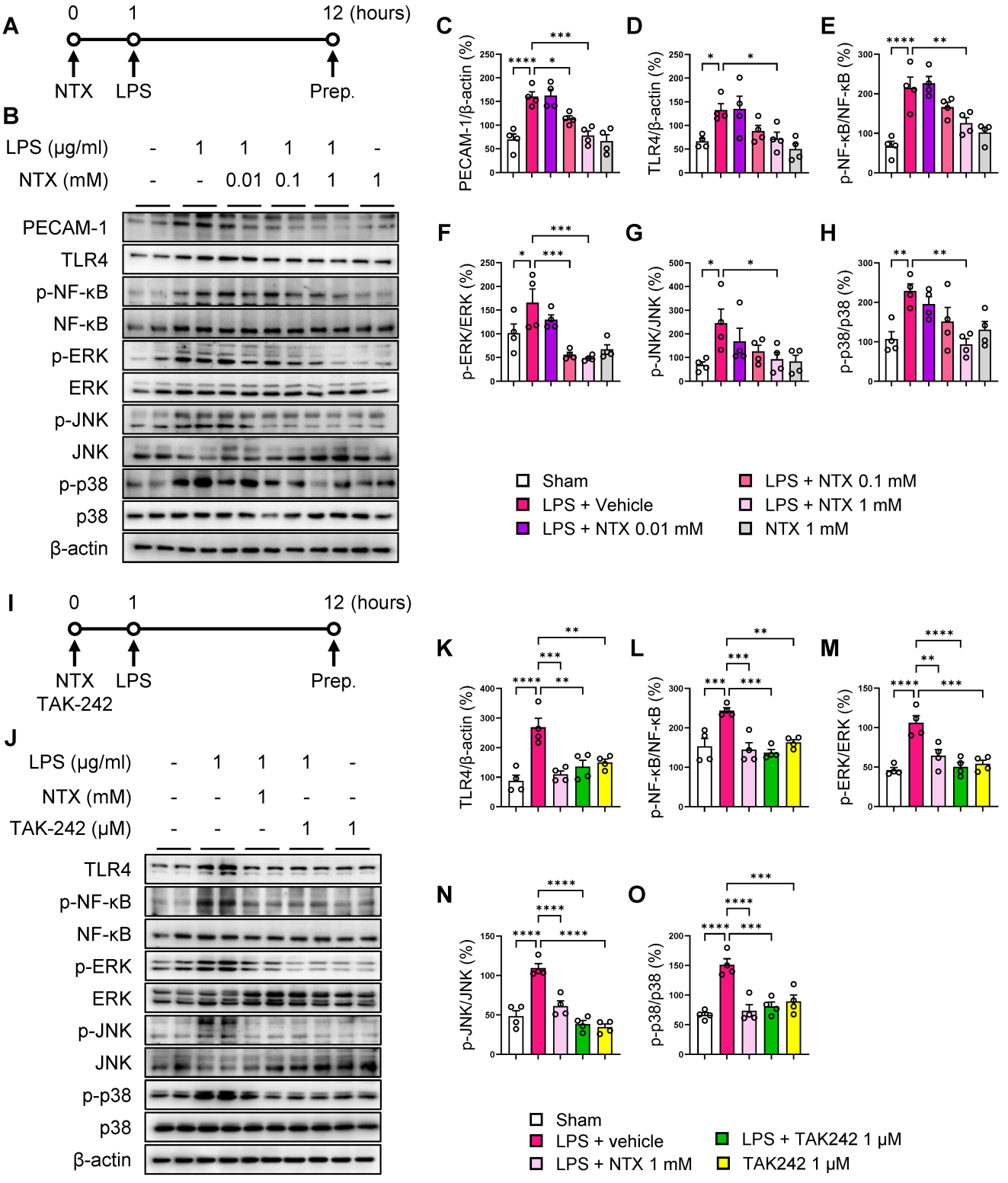


Figure 9. Naltrexone suppresses TLR4-associated NF-κB/MAPK signaling in bEnd.3 brain endothelial cells. (A) Schematic overview of the experimental design. bEnd.3 mouse brain endothelial cells were pretreated with naltrexone (NTX; 0.01, 0.1, or 1 mM) for 1 h before lipopolysaccharide (LPS; 5 μg/mL) stimulation and harvested 12 h later for protein analysis. **(B)** Representative Western blot images of PECAM-1, TLR4, and phosphorylated and total NF-κB p65, ERK, JNK, and p38. β-Actin was used as a loading control. **(C, D)** Densitometric quantification of PECAM-1 (C) and TLR4 (D) protein levels normalized to β-actin. **(E–H)** Densitometric quantification of the phosphorylation ratios of NF-κB p65 (E), ERK (F), JNK (G), and p38 (H), normalized to their corresponding total protein levels. **(I)** Schematic overview of the experimental design for pharmacological assessment of TLR4 involvement using TAK-242. bEnd.3 cells were pretreated with NTX (1 mM) or TAK-242 (1 μg/mL) for 1 h before LPS stimulation and harvested 12 h later for protein analysis. **(J)** Representative Western blot images of TLR4 and phosphorylated and total NF-κB p65, ERK, JNK, and p38. β-Actin was used as a loading control. **(K)** Densitometric quantification of TLR4 protein levels normalized to β-actin. **(L–O)** Densitometric quantification of the phosphorylation ratios of NF-κB p65 (L), ERK (M), JNK (N), and p38 (O), normalized to their corresponding total protein levels. Data are presented as mean ± SEM (n = 3 independent experiments). **P* < 0.05, ***P* < 0.01, ****P* < 0.001, and *****P* < 0.0001.

Supporting the potential involvement of opioid receptor-related mechanisms, naltrexone-mediated opioid receptor antagonism has been reported to modulate inflammatory responses in certain experimental settings, including cytokine production and NF-κB and MAPKs signaling [37]. In addition, chronic naltrexone administration has been shown to alter opioid receptor feedback mechanisms in immune cells [38]. Together, these observations suggest that sustained systemic exposure may engage complex opioid receptor-associated immune responses that could influence the net therapeutic effect of naltrexone *in vivo* [37, 38].

To investigate whether enhanced MOR antagonism contributes to the diminished efficacy of high-dose IVL4002, MNTX which is generally classified as a peripherally acting MOR antagonist, was administered at 3 mg/kg/day, a dose within the pharmacologically active range reported in mice [39]. MNTX co-administration had little effect on the efficacy of IVL4002 at 1 mg/head but partially restored the diminished efficacy observed at 10 mg/head. These findings do not support a simple model in which enhanced peripheral MOR antagonism alone accounts for the bell-shaped dose–response relationship. Nevertheless, MOR involvement cannot be excluded because MNTX has substantially lower MOR-binding affinity than naltrexone, with an approximately 40-fold difference reported in a direct receptor-binding comparison [40, 41], and receptor occupancy was not measured. Although MNTX is generally classified as a peripherally acting MOR antagonist [40, 42], MNTX and its demethylated metabolite naltrexone may reach the brain in mice [39], limiting attribution of its effects exclusively to peripheral MOR antagonism. The non-monotonic response may therefore reflect complex exposure-dependent interactions between opioid receptor signaling, the non-opioid immunomodulatory effects of naltrexone, and other compensatory physiological responses. In addition, the naltrexone concentrations used in the *in vitro* experiments were substantially higher than the plasma concentrations achieved following IVL4002 administration *in vivo*. Accordingly, the concentration-dependent effects observed *in vitro* should not be interpreted as directly equivalent to the exposure–efficacy relationship observed *in vivo*. Future studies should evaluate the effects of naltrexone at lower, physiologically relevant concentrations and determine drug exposure in relevant tissues. Direct assessment of MOR occupancy and downstream inflammatory signaling will also be required to clarify the mechanism underlying the non-monotonic dose–response relationship.

A defining feature of EAE pathogenesis is the activation and expansion of autoreactive $CD4^+$ T cells—particularly Th1 and Th17 subsets—in secondary lymphoid organs, followed by their migration into the CNS [32, 43, 44]. In the present study, IVL4002 selectively reduced splenic and lymph node hypertrophy and decreased $CD4^+$ Th1 and Th17 populations without substantially affecting $CD8^+$ T cells, suggesting preferential modulation of pathogenic $CD4^+$ T-cell responses rather than generalized suppression of T-cell populations. Flow cytometric analyses demonstrated reduced Th1 and Th17 cell infiltration into the lumbar spinal cord, and these findings were further corroborated by immunofluorescence staining, which provided direct spatial evidence of reduced accumulation of pathogenic Th1 and Th17 cells within inflammatory spinal cord lesions. Together, these findings suggest that IVL4002 limits the peripheral expansion and subsequent CNS accumulation of encephalitogenic T cells, thereby contributing to the attenuation of CNS inflammation in EAE [44].

Within the CNS, IVL4002 markedly suppressed inflammatory cell infiltration, reduced microglial/macrophage activation, attenuated reactive astrogliosis, and preserved myelin integrity in the lumbar spinal cord. Chronic microglial activation is increasingly recognized as an important contributor to persistent neuroinflammation and tissue injury in MS, with activated microglia and astrocytes amplifying inflammatory responses within the CNS [3]. Consistent with these histopathological changes, IVL4002 reduced the expression of inflammatory mediators and suppressed TLR4/MyD88–NF-κB/MAPK signaling in the lumbar spinal cord. TLR4 is an important innate immune receptor implicated in MS and EAE and activates MyD88-dependent NF-κB and MAPK pathways that promote inflammatory responses [35, 45]. Complementary experiments in BV2 microglial cells showed that naltrexone attenuated LPS-induced microglial activation together with TLR4-associated NF-κB and MAPK signaling. Pharmacological inhibition of TLR4 with TAK-242 produced a similar pattern of suppression, providing additional evidence for the involvement of TLR4-associated signaling in the anti-inflammatory effects of naltrexone. Together, these *in vivo* and *in vitro* findings support the involvement of TLR4-associated innate immune signaling in the suppression of CNS inflammation by IVL4002. Previous studies have suggested that naltrexone and related compounds can modulate TLR4 signaling through interactions with its co-receptor MD-2 independently of classical opioid receptor activity [45, 46]. However, direct interaction of naltrexone with the MD-2/TLR4 complex was not examined in the present study. Therefore, our findings

support the involvement of TLR4-associated signaling but do not establish MD-2/TLR4 as a direct molecular target of naltrexone in this model.

BBB dysfunction is a central feature of MS and EAE pathology, facilitating the entry of circulating immune cells into the CNS and amplifying neuroinflammatory responses [2]. In the present study, IVL4002 markedly reduced Evans Blue extravasation and albumin leakage in the lumbar spinal cord while preserving the expression of the tight junction proteins CLDN5, OCLN, and ZO-1 and reducing PECAM-1 expression. Together, these functional and molecular findings provide complementary evidence that IVL4002 preserves BBB integrity during EAE. Consistent with these *in vivo* findings, naltrexone attenuated LPS-induced endothelial inflammatory responses and TLR4-associated NF-κB/MAPK signaling in bEnd.3 brain endothelial cells. Pharmacological inhibition of TLR4 with TAK-242 produced a similar pattern of suppression, further supporting the involvement of TLR4-associated signaling in endothelial inflammatory responses. These findings suggest that modulation of endothelial inflammatory signaling may contribute to the BBB-protective effects of IVL4002. However, the bEnd.3 monoculture model does not fully recapitulate the multicellular complexity of the BBB [47, 48], and direct interaction of naltrexone with endothelial MD-2/TLR4 was not examined in the present study. Thus, the endothelial findings provide mechanistic support for, but do not establish, a direct endothelial mechanism underlying BBB protection by IVL4002. Collectively, preservation of BBB integrity may contribute to reduced CNS immune-cell infiltration and attenuation of neuroinflammatory pathology in EAE.

The sustained-release formulation represents an important pharmacological feature of IVL4002. Pharmacokinetic analysis confirmed sustained plasma exposure following a single subcutaneous administration of IVL4002 in mice, with systemic exposure increasing in a dose-dependent manner. In the EAE model, the greatest therapeutic efficacy was observed at 1 mg/head, corresponding to a plasma concentration range of approximately 0.16–3.19 ng/mL and an average plasma concentration of approximately 1.39 ng/mL. In clinical practice, oral naltrexone administered at 50 mg/day for substance use disorders has been reported to produce plasma concentrations of approximately 8.6 ng/mL (C_max) and 3–5 ng/mL (C_avg) [49]. Although direct cross-species comparisons should be interpreted cautiously, these findings indicate that therapeutic efficacy in EAE was achieved at systemic naltrexone concentrations lower than those reported with standard oral dosing in humans. Importantly, the therapeutic efficacy observed following a single administration was maintained throughout the 60-day observation period, further supporting the potential of IVL4002 to provide sustained pharmacological benefit without repeated dosing. Oral naltrexone undergoes extensive first-pass hepatic metabolism and exhibits substantial interindividual variability in systemic exposure [50]. By providing sustained systemic exposure after a single administration, IVL4002 may reduce dosing frequency and treatment burden, potentially offering an advantage for long-term therapy in which adherence is an important consideration [51, 52]. However, adherence was not directly evaluated in the present study, and this potential clinical advantage remains to be established.

The IVL-DrugFluidic® platform allows precise control of formulation parameters, including microparticle size distribution and polymer composition, which can influence drug-release characteristics. IVL4002 exhibited a narrow and uniform particle-size distribution, an important formulation characteristic for reproducible drug release. Because particle size can influence initial burst release, subsequent release kinetics, and injectability [19], the controlled particle characteristics of IVL4002 provide a formulation basis for sustained and reproducible drug delivery.

The translational potential of IVL4002 is further supported by its nonclinical safety profile. In GLP toxicology studies, repeated high-dose administration of IVL4002 did not produce treatment-related systemic toxicity in rats or dogs. Histopathological evaluation of injection sites revealed mild granulomatous inflammation in both placebo microsphere- and IVL4002-treated animals, with mild mixed inflammatory cell infiltration and focal hemorrhage additionally observed in the rat single-dose IVL4002 group (Figure S1). No severe inflammation, tissue necrosis, or other adverse local pathological changes were identified. Mild granulomatous inflammation is a recognized foreign-body response to biodegradable polyester materials [53]. Because similar granulomatous changes were observed in both placebo microsphere- and IVL4002-treated animals, these findings were considered more consistent with a local response to the biodegradable PLGA microspheres than with naltrexone-specific toxicity. Collectively, these findings support the local tolerability and favorable nonclinical safety profile of IVL4002. From a translational perspective, safety and tolerability remain important considerations in the long-term treatment of MS, as currently used oral disease-modifying therapies are associated with clinically relevant adverse effects; DMF is commonly

associated with flushing and gastrointestinal adverse events, whereas teriflunomide has been associated with hepatic and other systemic adverse events [54, 55]. Importantly, the present study was not designed to directly compare the safety of IVL4002 with these disease-modifying therapies, and such comparisons cannot be inferred from the current data. Together with the sustained pharmacokinetic exposure and durable efficacy following a single administration, the GLP toxicology findings provide an important preclinical basis for further translational development of IVL4002. Moreover, because naltrexone is an approved drug with an established clinical safety profile [56], its reformulation as a long-acting injectable may facilitate its repurposing for a new therapeutic indication. Further studies are warranted to characterize long-term injection-site responses and determine whether the sustained pharmacological and therapeutic effects observed in EAE translate into clinical benefit in MS.

Several limitations of this study should be acknowledged. First, although IVL4002 is formulated using biodegradable PLGA polymers that undergo hydrolytic degradation into lactic acid and glycolic acid, which are subsequently metabolized through endogenous pathways [19, 57], the biodistribution, degradation kinetics, and clearance of IVL4002 microspheres were not directly evaluated. Future studies using appropriately labeled microspheres will be important to characterize their biodistribution, degradation kinetics, and *in vivo* fate. Second, the relative contributions of opioid receptor-dependent and TLR4-associated mechanisms to the therapeutic effects of IVL4002 remain incompletely defined. Although the MNTX experiments suggest that peripheral MOR signaling may contribute to the differential efficacy observed across IVL4002 doses, they do not fully resolve the respective contributions of opioid receptor and TLR4-associated mechanisms. Moreover, the consequences of prolonged opioid receptor modulation associated with sustained naltrexone exposure warrant further investigation. Third, the present study was conducted in a single EAE model. Although MOG_{35-55}-induced EAE in C57BL/6 mice reproducibly exhibits key pathological features relevant to MS, including T cell-mediated neuroinflammation, demyelination, glial activation, BBB dysfunction, and neurological deficits [3, 58, 59], it does not recapitulate the heterogeneous clinical courses of human MS [58]. Future studies using complementary EAE models, including PLP-induced EAE in SJL mice and MOG-induced EAE in NOD mice, will be important to determine whether the therapeutic effects of IVL4002 extend to relapsing and progressive disease settings.

Despite these limitations, the present study provides preclinical evidence that sustained naltrexone delivery through IVL4002 produces durable therapeutic effects in EAE while modulating peripheral pathogenic T-cell responses, CNS inflammation, and BBB dysfunction. Together with its sustained pharmacokinetic profile and favorable nonclinical safety findings, these results support further investigation of IVL4002 as a long-acting therapeutic strategy for MS.

Conclusions

In conclusion, this study demonstrates that a single administration of IVL4002, a sustained-release naltrexone microsphere formulation, provides durable therapeutic efficacy in EAE, with maximal benefit achieved within an effective systemic exposure range. IVL4002 coordinately attenuated peripheral pathogenic Th1/Th17 responses and their CNS infiltration, suppressed glial and TLR4/MyD88–NF-κB/MAPK-associated inflammatory signaling, and preserved BBB integrity, thereby limiting neuroinflammation, demyelination, and neurological disease severity. Importantly, therapeutic efficacy was maintained throughout the 60-day observation period, while pharmacokinetic and nonclinical safety findings further supported the long-acting therapeutic profile of IVL4002. Collectively, these findings provide a preclinical basis for further investigation of IVL4002 as a long-acting naltrexone repurposing strategy for MS.

Abbreviations

BBB: blood–brain barrier; BV2: murine microglial cell line; CNS: central nervous system; DMF: dimethyl fumarate; EAE: experimental autoimmune encephalomyelitis; ERK: extracellular signal–regulated kinase; GFAP: glial fibrillary acidic protein; H&E: hematoxylin and eosin; IFN-γ: interferon gamma; IL-17A: interleukin-17A; IL-6: interleukin-6; iNOS: inducible nitric oxide synthase; JNK: c-Jun N-terminal kinase; LAI: long-acting injectable; LPS: lipopolysaccharide; MAPKs: mitogen-activated protein kinases; MBP: myelin basic protein; MD-2: myeloid differentiation factor-2; MS: multiple sclerosis; NF-κB: nuclear factor kappa B; NTX: naltrexone; PECAM-1: platelet endothelial cell adhesion molecule-1; RT-PCR: reverse transcription polymerase chain reaction; SEM: scanning electron microscopy; SSC: side scatter; TLR4: Toll-like receptor 4.

Supplementary Material

Supplementary figures and tables.
https://www.thno.org/v17p0671s1.pdf

Acknowledgements

Financial support

The study was supported by InventageLab Inc. Employees of the sponsor contributed to the study as described in the Author Contributions section. All scientific conclusions were based on the authors' interpretation of the data, and all authors approved the final version of the manuscript.

Ethics approval and consent to participate

All animal experiments were conducted in accordance with the guidelines for the care and use of laboratory animals and were approved by the Institutional Animal Care and Use Committee (IACUC) of BIOSTEP Co., Ltd. (Approval No. BIOSTEP 25-HB-0017), the IIT Research Institute (IITRI) (Approval Nos. IITRI 311900100201 and IITRI 311900100301), and Kyung Hee University (Approval No. KHUASP(SE)-23-560). All procedures were performed in accordance with institutional and national guidelines and were designed to minimize animal suffering.

Availability of data and materials

The datasets generated and/or analyzed during the current study are available from the corresponding author on reasonable request.

Author contributions

TWK performed conceptualization, formal analysis, investigation, validation, visualization, and writing – original draft. SY contributed to conceptualization formal analysis, investigation, validation, visualization and writing – original draft. HSJ, YH, and DP conducted investigation, validation, and visualization. SL contributed to conceptualization, formal analysis, investigation, and validation. YL performed formal analysis, visualization and writing – original draft. JC was responsible for project administration. JK contributed to conceptualization, supervision, project administration, and writing – review & editing. IHC contributed to conceptualization, funding acquisition, resources, supervision, project administration, and writing – review & editing. All authors read and approved the final manuscript.

Artificial Intelligence (AI) Usage Statement

Generative AI tools were used solely for English-language editing to improve grammar, clarity, and readability. All AI-assisted text was reviewed and verified by the authors, who take full responsibility for the manuscript.

Competing Interests

The authors have declared that no competing interest exists.

References

1. Kuhlmann T, Moccia M, Coetzee T, Cohen JA, Correale J, Graves J, et al. Multiple sclerosis progression: time for a new mechanism-driven framework. Lancet Neurol. 2023; 22: 78–88.
2. Zierfuss B, Larochelle C, Prat A. Blood-brain barrier dysfunction in multiple sclerosis: causes, consequences, and potential effects of therapies. Lancet Neurol. 2024; 23: 95–109.
3. Distéfano-Gagné F, Bitarafan S, Lacroix S, Gosselin D. Roles and regulation of microglia activity in multiple sclerosis: insights from animal models. Nat Rev Neurosci. 2023; 24: 397–415.
4. Nishihara H, Perriot S, Gastfriend BD, Steinfort M, Cibien C, Soldati S, et al. Intrinsic blood-brain barrier dysfunction contributes to multiple sclerosis pathogenesis. Brain. 2022; 145: 4334–48.
5. Kołtuniuk A, Rosińczuk J. Adherence to disease-modifying therapies in patients with multiple sclerosis. Patient Prefer Adherence. 2018; 12: 1557–66.
6. Gerber B, Cowling T, Chen G, Yeung M, Duquette P, Haddad P. The impact of treatment adherence on clinical and economic outcomes in multiple sclerosis: Real world evidence from Alberta, Canada. Mult Scler Relat Disord. 2017; 18: 218–24.
7. Dabi YT, Ajagbe AO, Degechisa ST. Toll-like receptors in pathogenesis of neurodegenerative diseases and their therapeutic potential. Immun Inflamm Dis. 2023; 11: e839.
8. Wang Y, Wu T, Tsai M-C, Rezzonico MG, Abdel-Haleem AM, Xie L, et al. TPL2 kinase activity regulates microglial inflammatory responses and promotes neurodegeneration in tauopathy mice. eLife. 2023; 12: e83451.
9. Zhang W, Xiao D, Mao Q, Xia H. Role of neuroinflammation in neurodegeneration development. Signal Transduct Target Ther. 2023; 8: 267.
10. Miranda-Hernandez S, Baxter AG. Role of toll-like receptors in multiple sclerosis. Am J Clin Exp Immunol. 2013; 2: 75–93.
11. Broglio K, Matzo M. CE: Acute Pain Management for People with Opioid Use Disorder. Am J Nurs. 2018; 118: 30–8.
12. Wang X, Zhang Y, Peng Y, Hutchinson MR, Rice KC, Yin H, et al. Pharmacological characterization of the opioid inactive isomers (+)-naltrexone and (+)-naloxone as antagonists of toll-like receptor 4. Br J Pharmacol. 2016; 173: 856–69.
13. Younger J, Parkitny L, McLain D. The use of low-dose naltrexone (LDN) as a novel anti-inflammatory treatment for chronic pain. Clin Rheumatol. 2014; 33: 451–9.
14. Cree BA, Kornyeyeva E, Goodin DS. Pilot trial of low-dose naltrexone and quality of life in multiple sclerosis. Ann Neurol. 2010; 68: 145–50.
15. Li Z, You Y, Griffin N, Feng J, Shan F. Low-dose naltrexone (LDN): A promising treatment in immune-related diseases and cancer therapy. Int Immunopharmacol. 2018; 61: 178–84.
16. Gironi M, Martinelli-Boneschi F, Sacerdote P, Solaro C, Zaffaroni M, Cavarretta R, et al. A pilot trial of low-dose naltrexone in primary progressive multiple sclerosis. Mult Scler. 2008; 14: 1076–83.
17. Ludwig MD, Turel AP, Zagon IS, McLaughlin PJ. Long-term treatment with low dose naltrexone maintains stable health in patients with multiple sclerosis. Mult Scler J Exp Transl Clin. 2016; 2: 2055217316672242.
18. Sharafaddinzadeh N, Moghtaderi A, Kashipazha D, Majdinasab N, Shalbafan B. The effect of low-dose naltrexone on quality of life of patients with multiple sclerosis: a randomized placebo-controlled trial. Mult Scler. 2010; 16: 964–9.
19. Makadia HK, Siegel SJ. Poly Lactic-co-Glycolic Acid (PLGA) as Biodegradable Controlled Drug Delivery Carrier. Polymers (Basel). 2011; 3: 1377–97.
20. Fredenberg S, Wahlgren M, Reslow M, Axelsson A. The mechanisms of drug release in poly(lactic-co-glycolic acid)-based drug delivery systems--a review. Int J Pharm. 2011; 415: 34–52.
21. Landis SC, Amara SG, Asadullah K, Austin CP, Blumenstein R, Bradley EW, et al. A call for transparent reporting to optimize the predictive value of preclinical research. Nature. 2012; 490: 187–91.
22. Choi JH, Oh J, Lee MJ, Ko SG, Nah SY, Cho IH. Gintonin mitigates experimental autoimmune encephalomyelitis by stabilization of Nrf2 signaling via stimulation of lysophosphatidic acid receptors. Brain Behav Immun. 2021; 93: 384–98.
23. Choi JH, Oh J, Lee MJ, Bae H, Ko SG, Nah SY, et al. Inhibition of lysophosphatidic acid receptor 1-3 deteriorates experimental autoimmune encephalomyelitis by inducing oxidative stress. J Neuroinflammation. 2021; 18: 240.
24. Yuan CS, Wang CZ, Attele A, Zhang L. Methylnaltrexone reduced body weight gain in ob/ob mice. J Opioid Manag. 2009; 5: 213–8.
25. Yamakita S, Fujita D, Sudo K, Ishikawa D, Kushimoto K, Horii Y, et al. Activation of neurons and satellite glial cells in the DRG produces morphine-induced hyperalgesia. Mol Pain. 2023; 19: 17448069231181973.
26. Lee MJ, Bing SJ, Choi J, Jang M, Lee G, Lee H, et al. IKKβ-mediated inflammatory myeloid cell activation exacerbates experimental autoimmune encephalomyelitis by potentiating Th1/Th17 cell activation and compromising blood brain barrier. Mol Neurodegener. 2016; 11: 54.

27. Kuo PC, Weng WT, Scofield BA, Paraiso HC, Brown DA, Wang PY, et al. Dimethyl itaconate, an itaconate derivative, exhibits immunomodulatory effects on neuroinflammation in experimental autoimmune encephalomyelitis. J Neuroinflammation. 2020; 17: 138.
28. Kwon TW, Ha Y, Jo HS, Cho IH. Regional and Cell-Type-Specific Activation of YAP/TAZ Underlies Glial Responses in LPS-Induced Neuroinflammation. Glia. 2026; 74: e70129.
29. Oh J, Kwon TW, Choi JH, Kim Y, Moon SK, Nah SY, et al. Ginsenoside-Re inhibits experimental autoimmune encephalomyelitis as a mouse model of multiple sclerosis by downregulating TLR4/MyD88/NF-κB signaling pathways. Phytomedicine. 2024; 122: 155065.
30. Lee HG, Rone JM, Lee JH, Quintana FJ. Glial cells in chronic inflammation: diversity, dysfunction and therapeutic targeting. Nat Rev Immunol. 2026.
31. Tsunoda I, Libbey JE, Kuang LQ, Terry EJ, Fujinami RS. Massive apoptosis in lymphoid organs in animal models for primary and secondary progressive multiple sclerosis. Am J Pathol. 2005; 167: 1631–46.
32. Constantinescu CS, Farooqi N, O'Brien K, Gran B. Experimental autoimmune encephalomyelitis (EAE) as a model for multiple sclerosis (MS). Br J Pharmacol. 2011; 164: 1079–106.
33. Mustafa AM, Shaheen AM, Zaki HF, Rabie MA. Nicorandil and carvedilol mitigates motor deficits in experimental autoimmune encephalomyelitis-induced multiple sclerosis: Role of TLR4/TRAF6/MAPK/NF-κB signalling cascade. Int Immunopharmacol. 2024; 127: 111387.
34. Jingjing H, Tongqian W, Shirong Y, Lan M, Jing L, Shihui M, et al. S100A4 promotes experimental autoimmune encephalomyelitis by impacting microglial inflammation through TLR4/NF-κB signaling pathway. Int Immunopharmacol. 2024; 142: 112849.
35. Asadzadeh Manjili F, Yousefi-Ahmadipour A, Kazemi Arababadi M. The roles played by TLR4 in the pathogenesis of multiple sclerosis; A systematic review article. Immunol Lett. 2020; 220: 63–70.
36. Attfield KE, Jensen LT, Kaufmann M, Friese MA, Fugger L. The immunology of multiple sclerosis. Nat Rev Immunol. 2022; 22: 734–50.
37. Hutchinson MR, Bland ST, Johnson KW, Rice KC, Maier SF, Watkins LR. Opioid-induced glial activation: mechanisms of activation and implications for opioid analgesia, dependence, and reward. ScientificWorldJournal. 2007; 7: 98–111.
38. Pandey V, Yadav V, Srivastava A, Gaglani P, Singh R, Subhashini. Blocking μ-opioid receptor by naltrexone exaggerates oxidative stress and airway inflammation via the MAPkinase pathway in a murine model of asthma. Free Radic Biol Med. 2024; 212: 94–116.
39. Walentiny DM, Komla E, Moisa LT, Mustafa MA, Poklis JL, Akbarali HI, et al. Methylnaltrexone crosses the blood-brain barrier and attenuates centrally-mediated behavioral effects of morphine and oxycodone in mice. Neuropharmacology. 2021; 185: 108437.
40. Yuan CS, Israel RJ. Methylnaltrexone, a novel peripheral opioid receptor antagonist for the treatment of opioid side effects. Expert Opin Investig Drugs. 2006; 15: 541–52.
41. Yuan CS. Methylnaltrexone mechanisms of action and effects on opioid bowel dysfunction and other opioid adverse effects. Ann Pharmacother. 2007; 41: 984–93.
42. Viscusi ER, Viscusi AR. Blood-brain barrier: mechanisms governing permeability and interaction with peripherally acting μ-opioid receptor antagonists. Reg Anesth Pain Med. 2020; 45: 688–95.
43. Song Y, Li J, Wu Y. Evolving understanding of autoimmune mechanisms and new therapeutic strategies of autoimmune disorders. Signal Transduct Target Ther. 2024; 9: 263.
44. Rudnicka-Czerwiec J, Bartosik-Psujek H. Innate Immunity in the Pathogenesis of Selected Autoimmune Neurological Diseases. J Clin Med. 2025; p. 7235.
45. Zhang P, Yang M, Chen C, Liu L, Wei X, Zeng S. Toll-Like Receptor 4 (TLR4)/Opioid Receptor Pathway Crosstalk and Impact on Opioid Analgesia, Immune Function, and Gastrointestinal Motility. Front Immunol. 2020; 11: 1455.
46. Selfridge BR, Wang X, Zhang Y, Yin H, Grace PM, Watkins LR, et al. Structure–Activity Relationships of (+)-Naltrexone-Inspired Toll-like Receptor 4 (TLR4) Antagonists. J Med Chem. 2015; 58: 5038–52.
47. Watanabe T, Dohgu S, Takata F, Nishioku T, Nakashima A, Futagami K, et al. Paracellular barrier and tight junction protein expression in the immortalized brain endothelial cell lines bEND.3, bEND.5 and mouse brain endothelial cell 4. Biol Pharm Bull. 2013; 36: 492–5.
48. Li G, Simon MJ, Cancel LM, Shi ZD, Ji X, Tarbell JM, et al. Permeability of endothelial and astrocyte cocultures: in vitro blood-brain barrier models for drug delivery studies. Ann Biomed Eng. 2010; 38: 2499–511.
49. Shen PT, Liu SC, Huang MC, Liu YL. Development of a liquid chromatography-tandem mass spectrometry method for the analysis of plasma naltrexone and its active metabolite in patients with AUD. Eur J Mass Spectrom (Chichester). 2025; 31: 161–8.
50. Brünen S, Bekier NK, Hiemke C, Korf F, Wiedemann K, Jahn H, et al. Therapeutic Drug Monitoring of Naltrexone and 6β-Naltrexol During Anti-craving Treatment in Alcohol Dependence: Reference Ranges. Alcohol Alcohol. 2019; 54: 51–5.
51. Thapa Magar K, Boucetta H, Zhao Z, Xu Y, Liu Z, He W. Injectable long-acting formulations (ILAFs) and manufacturing techniques. Expert Opin Drug Deliv. 2024; 21: 881–904.
52. Santoleri F, Lasala R, Berardini E, Vernacchio F, Leo D, Costantini A. Adherence, Persistence, Switching and Costs of Injectable and Oral Therapies for Multiple Sclerosis. Real Life Analysis Over 6 Years of Treatment. Hosp Pharm. 2024; 59: 476–84.
53. Nonhoff M, Puetzler J, Hasselmann J, Fobker M, Gosheger G, Schulze M. The Potential for Foreign Body Reaction of Implanted Poly-L-Lactic Acid: A Systematic Review. Polymers (Basel). 2024; 16(6): 817.
54. Ali HT, Yousef AM, El-Farargy SH, Abdelmonhem AM, Abouda DA, Mahmoud AM, et al. An updated systematic review and meta-analysis exploring the efficacy and safety of dimethyl fumarate (DMF) for patients with multiple sclerosis (MS). BMJ Neurol Open. 2024; 6: e000872.
55. Ng HS, Zhu F, Zhao Y, Yao S, Lu X, Ekuma O, et al. Adverse Events Associated With Disease-Modifying Drugs for Multiple Sclerosis: A Multiregional Population-Based Study. Neurology. 2024; 102: e208006.
56. Bolton M, Hodkinson A, Boda S, Mould A, Panagioti M, Rhodes S, et al. Serious adverse events reported in placebo randomised controlled trials of oral naltrexone: a systematic review and meta-analysis. BMC Med. 2019; 17: 10.
57. Danhier F, Ansorena E, Silva JM, Coco R, Le Breton A, Préat V. PLGA-based nanoparticles: an overview of biomedical applications. J Control Release. 2012; 161: 505–22.
58. Lassmann H, Bradl M. Multiple sclerosis: experimental models and reality. Acta Neuropathol. 2017; 133: 223–44.
59. Bonaldo B, Casile A, Montarolo F, Bertolotto A. Modeling Multiple Sclerosis in the Two Sexes: MOG35-55-Induced Experimental Autoimmune Encephalomyelitis. J Vis Exp. 2023.